COO-2107-9

Contract AT(11-1)-2107

CORRELATION OF SUBSTRUCTURE WITH MECHANICAL PROPERTIES OF PLASTICALLY DEFORMED AISI 304 AND 316 STAINLESS STEEL

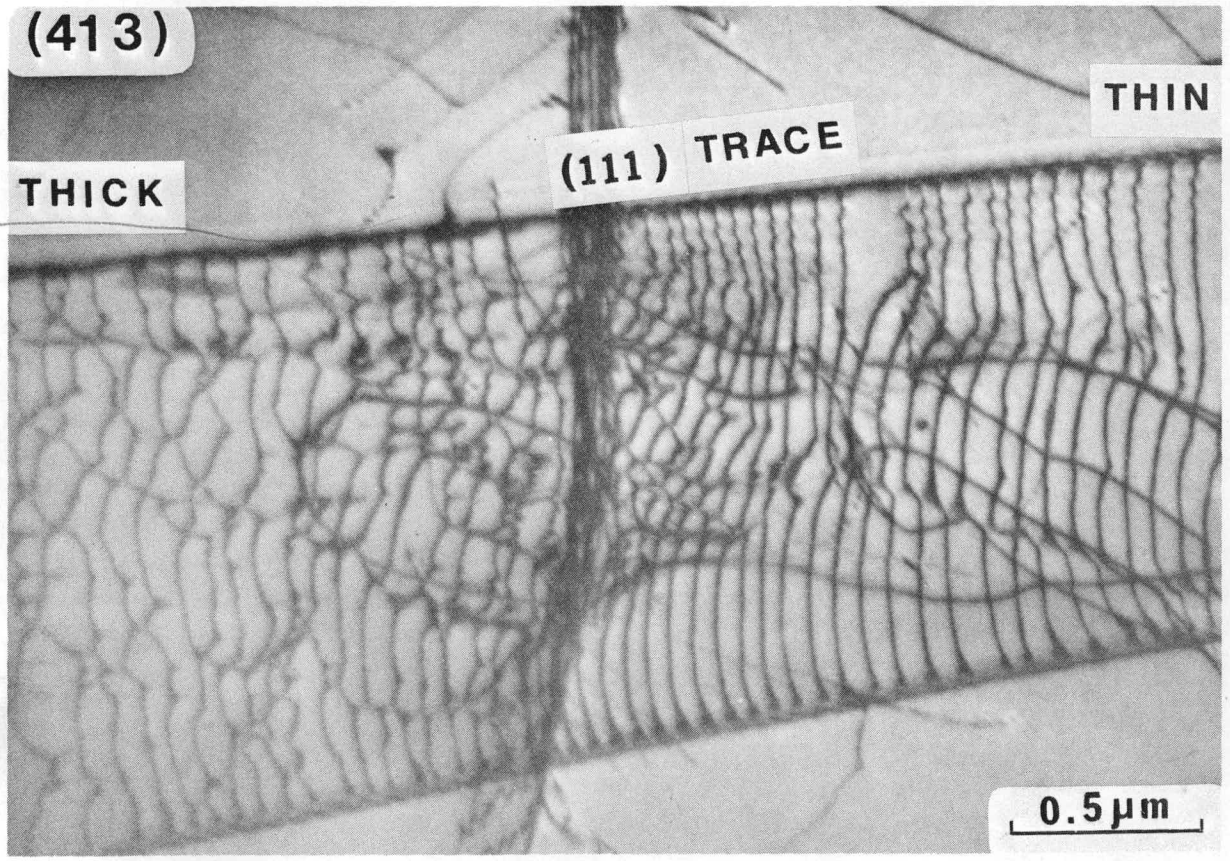

PROGRESS REPORT

Period January 1, 1973 to March 31, 1973

J. Moteff, Principal Investigator
Materials Science and Metallurgical Engineering Department

June 15, 1973

University of Cincinnati
Cincinnati, Ohio 45221

DISCLAIMER

TABLE OF CONTENTS

The transmission electron micrograph on the cover of this report is from a type 304L stainless steel tensile specimen tested in argon at 1000°C. The picture shows the arrangement of dislocations lying on (111) plane which makes a shallow angle with the foil surface. In the thicker region of the foil (left) the dislocations are irregular and form nodes. In the thinner region (right) they tend to be straight and align themselves. The oscillatory effects at images of dislocations is very clearly demonstrated in the upper right portion of the figure.

LIST OF TABLES

LIST OF FIGURES

SUMMARY

The recovery behavior of AISI 316 stainless steel specimens which have been cold-worked at 20, 35 and 50 percent has been studied using hot hardness measurements. It is shown that 50 percent cold-worked yields complete recovery at 900°C, while 35 and 20 percent produce only 88 and 69 percent recovery. The percent recovery has been shown to increase linearly with the increase in percent cold-work. The recovery behavior of stainless steel deformed to different degrees of cold-work is discussed in terms of stored energy and stabilization of the substructure by $M_{23}C_6$ type precipitates.

The hot hardness data on sixteen different heats of AISI 304 stainless steels have been reported. The hot hardness data on eight of the sixteen different heats have been correlated with the hot tensile data. The ultimate tensile strength, (σ_u), has been calculated using the equation,

$$\sigma_u = \frac{H}{3.1}\left(\frac{n}{0.217}\right)^n$$

and compared with the experimental values. The parameters H and n represent the microhardness and strain hardening exponent respectively.

Transmission electron microscopy (TEM) on eight of the sixteen different heats of AISI 304 stainless steels has been completed. Typical micrographs showing isolated and network of

extended nodes are presented.

Substructure of AISI 304L stainless steel tested in tensile up to 1375°C have been presented. The room temperature deformation is characterized by planar slip and dislocation cells are shown to form at higher temperature. Dislocation cells are observed to rearrange to well defined subgrains at test temperatures > 600°C.

Substructure study on Incoloy 800, tensile tested at 800, 1000, 1200, 1300 and 1400°F at a constant strain rate have been presented. The results show that cells and subgrains form in the temperature range 1000-1400°F. At 1200°F dislocation cells were observed to transform into well defined subgrains. The dislocation cell intercept showed a stress dependence of -2 and the subgrain intercept of -1. The dislocation line density showed a stress dependency of 2. The substructural results on Incoloy 800 suggest that its behavior can be compared closely with 304 and 316 stainless steel.

I. OBJECTIVE

The objective of this program is to evaluate (a) the time, temperature and stress dependent properties of austenitic stainless steels, 316 and 304, (b) the relationship of these properties to the substructure as observed principally with a 200 kV transmission electron microscope and (c) contribution of grain boundary sliding to plastic deformation at high temperature. Special consideration has been given to operating conditions typical of LMFBR applications, including the knowledge that the radiation environment can influence the substructure of these metals leading to significant changes in the mechanical property behavior. Related substructure studies on other metals (nickel) and alloys (Incoloy 800) are also being investigated.

II. INTRODUCTION

Hot-hardness and metallography of AISI 316 stainless steel specimens which have been cold-worked at 20, 35 and 50 percent have been completed. It is shown that 50 percent cold-worked yields complete recovery at 900°C, while 35 and 20 percent produce only 88 and 69 percent recovery. The recovery behavior of stainless steel deformed to different degrees of cold-work is discussed in terms of stored energy and stabilization of substructure by $M_{23}C_6$ type precipitates.

From previous results on substructure evaluation of AISI 316 stainless steel resulting from the change in stress levels

during the creep test, new creep tests with large stress changes have been planned and are in progress.

Hot-hardness on sixteen different heats of AISI 304 stainless steels have been completed and some of the data correlated with hot-tensile data. The hot-hardness and hot-tensile data show an excellent correlation with a coefficient of 3.1. The ultimate strength, (σ_u), has been calculated using the equation

$$\sigma_u = \frac{H}{3.1}\left(\frac{n}{0.217}\right)^n$$

and compared with the experimental values. The parameters H and n represent the microhardness and strain-hardening exponent respectively.

Transmission Electron Microscopy (TEM) on eight of the sixteen different heats of AISI 304 stainless steels has been completed. The micrographs are being analyzed quantitatively for stacking fault energy variation with chemical composition.

Substructure study on AISI 304L stainless steel tested in tensile up to 1375°C have been partially completed. Some data on substructural features are presented. The raw data on grain boundary sliding in 304 stainless steel (Reference Heat 9T2796), tensile tested at 650°C have been collected and its computer analysis is in progress.

Substructure data on Incoloy 800, tensile tested at 800, 1000, 1200, 1300 and 1400°F have been completed. A preliminary

correlation of dislocation cell and/or subgrain intercept and of mobile dislocation line density with maximum tensile stress are presented.

Substructural evaluations on 270 nickel, creep tested in steady state from 0.3 to 0.55 T_m, have been initiated.

III. EXPERIMENTAL PROGRAM [J. Moteff and V.K. Sikka]

The presentation of the experimental program is subdivided into four parts using the material categories of 316 stainless steel, 304 stainless steel, Incoloy 800 alloys and 270 nickel.

A. 316 Stainless Steel [V.K. Sikka, C.C. Yu and T.A. Kenfield]

Work on 316 stainless steel is continuing in the following three areas:

1. Creep-Substructure Relationship
2. Effect of Changing Stress on Creep Behavior
3. Recovery Behavior of Cold-Work 316 Stainless Steel.

The program and the status of the work in each area is presented below.

1. Creep-Substructure Relationship - Some results on creep-substructure relationship were presented in the previous report. The substructure alteration due to the change in stress from initial stress suggested that more creep tests should be run, where stress is changed (decreased or increased) by 25-50 percent of the initial stress. Such tests are in progress and will be presented in the next report.

2. Effect of Changing Stress on Creep Behavior - As indicated above, the creep tests with large stress changes are in the process of completion. The creep tests are planned to run under the conditions listed in Table I. Substructure study on the samples with large stress changes will be started after the completion of these tests.

3. Recovery Behavior of Cold-Work 316 Stainless Steel - The recovery behavior of cold-worked 316 stainless steel was planned to follow by means of the following properties:

i) Hot-Hardness

ii) Room Temperature Hardness (following elevated temperature anneals)

iii) Isochronal Resistivity Annealing

iv) Transmission Electron Microscopy (TEM)

The hot-hardness measurements have already been completed, while other property measurements are still in progress.

Hot-Hardness

Test samples were prepared from two material sources,

(a) Annealed 316 stainless steel bar (0.625 inch round times 12 inches long) obtained from the PNL Reference Heat 65808, and

(b) Pre-rolled, 20 percent CW 316 stainless steel sheet specimen (0.020 inch thick) from Heat 65808.

Material II was left in its original conditions. Four sets of samples were then prepared from Material I to include the following conditions:

TABLE I

TEST CONDITIONS FOR CREEP AND SUBSTRUCTURE STUDY ON 316[a] STAINLESS STEEL

Test	Specimen Number	Temperature °F	Temperature °C	Applied Stress Initial Ksi	Applied Stress Final[b] Ksi	Comments
1	S-19	1350	732	25	25	Creep to Rupture
2	S-20	1350	732	25	14	Reduce Stress and Creep to Rupture
3	S-21	1350	732	14	25	Increase Stress and Creep to Rupture
4	S-22	1350	732	25	14	Stop Before Rupture

(a) Heat No. PNL 65808.

(b) Represents the stress changed from initial. The stress will be changed from first level to second when the creep process is in the steady-state.

Annealed Control

20 percent CW

35 percent CW

50 percent CW

Hot-hardness measurements were made on both Materials I (processed) and II. The hot-hardness samples were: 0.5 mm (0.020 inch) thick, 3/8 inch wide and 7/8 inch in length. All samples were electropolished using a solution of 90 percent acetic acid - 10 percent perchloric as an electrolyte.

The electropolished samples were placed in a hot-hardness furnace, which was evacuated to 5×10^{-5} torr. All measurements were made using a diamond pyramid hardness indenter. Three indents, with hold time of 30 seconds and using 500 gram load, were made at each temperature after the specimen soaked at the test temperature for approximately 30 minutes. The furnace atmosphere during the test was made of high purity argon gas. Details of the hot-hardness test assembly have been presented previously[1].

The test temperatures selected for hot-hardness measurements were in this order: Room Temperature, 100, 200, 250, 300, 350, 400, 500, 550, 600, 700, 800, 900, 750, 600, 200, 100°C and Room Temperature.

Metallography was done on both starting materials I and II. A typical micrograph of the annealed control material is shown

in Figure 1. The microstructure shows large grains containing annealing twins, the grain size of the starting material (Figure 1) corresponds to ASTM 5. Typical microstructures developed in Material I on cold-working are shown in Figures 2-4. The microstructure of 20 percent cold-worked sheet from Material II is shown in Figure 5. A comparison of cold-worked structure with the control annealed microstructure shows the development of a large amount of deformation twins. The amount of deformation twinning seems to increase with an increasing amount of cold-work. The microstructure of 20 percent cold-worked stainless steel sheet, Figure 5, shows a distinct difference in grain size as compared to 20 percent cold-worked bar, Figure 2. Both materials have the same room temperature hardenss. The 20 percent cold-worked bar has larger starting grain size and contains more annealing and deformation twins, while the 20 percent cold-worked sheet has smaller grain size and is virtually free of deformation twins. Thus, while the hardness of 20 percent cold-worked bar could be accounted for by deformation twins, the hardness of 20 percent sheet is probably due to smaller grain size.

Hot-hardness data on anneal control 316 stainless steel is shown in Figure 6. Similar hot-hardness curves for 20 percent cold-work sheet and bar are compared in Figure 7. Hot-hardness recovery curves for three different amounts of cold-work, 20, 35 and 50 percent on 316 bar stock are presented in Figure 8. In

general hot-hardness curves show a plateau up to 500°C and then show a continuous decrease in hardness to 900°C. The descending curve represents the hardness variation of partially or fully recovered samples. For annealed control samples, Figure 6, there is essentially no cold-work and so ascending and descending curves coincide with each other. In Figure 7, a comparison of recovery of 20 percent cold-worked bar and sheet specimens shows that within experimental scatter, there is no difference between the two. Figure 8 shows the amount of recovery obtained in three different cold-works. The recovery is maximum for 50 percent cold-work and minimum for 20 percent cold-work. Furthermore, a comparison of descending curve for 50 percent cold-work and that for anneal control material shows that there is complete recovery of the cold-work. Similar comparisons for 35 percent and 20 percent cold-work reveal that recovery for 20 percent cold-work is the minimum. Percent recovery can be calculated by the following relationship:

$$\% \text{ Recovery} = \left(\frac{H_A - H_B}{H_A - H_C}\right) X\ 100 \qquad (1)$$

where

H_A = Room temperature hardness in as cold-work condition.

H_B = Room temperature hardness in recovered condition.

H_C = Room temperature hardness for an anneal control sample.

The percent recovery calculation shows a 100 percent recovery for 50 percent cold-work and 67.5 percent for 20 percent cold-work. A variation of percent recovery with percent cold-work is shown in Figure 8. It is noted that percent recovery increases linearly with the percent cold-work.

The recovery behavior of cold-worked 316 stainless steel is governed by two important factors,

(a) Stored Energy, and

(b) Nulceation and Growth of Various Phases.

The amount of stored energy increases with the amount of cold-work and so one would expect 50 percent cold-work to contain much more than 20 percent cold-work. The amount of stored energy determines the driving force for the recovery process. Thus, if no new phases form during annealing, maximum recovery would be expected in 50 percent cold-work and minimum in 20 percent cold-work. Such a possibility is shown in Figure 8. But, Weiss and Stickler[2] and Spruiell et al.[3] have shown that ageing of cold-worked stainless steel produces various phases and so the direct effect of stored energy on recovery gets modified. Such modification of recovery behavior comes from the fact that various nucleating phases stabilize the substructure formed during cold-working.

Weiss and Stickler[2] have investigated the detailed crystal structure and indentification of various phases formed

during ageing cold-worked 316 stainless steel and their results are presented in Table II. Weiss and Stickler[2] have gone through extraction of various phases as a function of ageing time and plotted a time - temperature - precipitation diagram. A typical time - temperature - precipitation diagram for 316 L (0.023% C) is shown[1] in Figure 9. The accelerating effect of cold-work on precipitation kinetics is shown by the shift of the curve to the left. Figure 10 shows[3] a typical curve for bulk extracted residue as a function of time at 710°C for 316 (0.060% C) for 20 percent and 50 percent cold-work. It can be seen that the amount of precipitate for the same time is almost 20 times greater in 50 percent cold-worked stainless steel than in 20 percent cold worked. The precipitate kinetics given in Figure 10 suggest that precipitates should be much larger in size for 50 percent cold-work than for 20 percent cold-work. The large precipitates in 50 percent cold-work will be less effective in stabilizing the substructure compared to smaller numerous precipitates in 35 and 20 percent cold-work samples. Thus, the recovery in 50 percent cold-work is still dominated by its stored energy, whereas in the cases of 35 and 20 percent cold-work, stored energy contribution to recovery would be reduced by the effective stabilization of the substructure by small precipitates ($M_{23}C_6$, M_6C, σ, η and χ). Thus, recovery would be expected to

TABLE II

CRYSTAL STRUCTURE AND COMPOSITION OF PHASES IN AGED TYPE 316L AND 316 STAINLESS STEELS (REF. 2)

Phase	Crystal Structure	Lattice Parameters		Composition, Wt Pct, Determined by Energy-Dispersive X-ray Spectroscopy							
		This Investigation	Literature [Ref.]	This Investigation				Literature [Ref.]			
$M_{23}C_6$	fcc	a_0 = 10.569(650°C for 1500 hr) to a_0 = 10.676(900°C for 150 hr)	a_0 = 10.680[8] a_0 = 10.638[24] [25] a_0 = 10.62[27]	Mo 14	Cr 63	Fe 18	Ni 5	$(Cr_{17}Fe_{4.5}Mo_{1.5})C_6$ [8] $(FeCr)_{23}C_6$ [24]			
				$(Cr_{16}Fe_5Mo_2)C_6$							
M_6C	fcc	a_0 = 10.95 ± 0.01	a_0 = 10.85[61] a_0 = 11.11[25]					(Cr, Co, Mo, Ni)$_6$C[61] Fe_3Mo_3C[35]			
Sigma (σ)	Tetragonal	a_0 = 8.828 ± 0.001 c_0 = 4.597 ± 0.001(815°C for 3000 hr) a_0 = 8.832 ± 0.001 c_0 = 4.599 ± 0.001(900°C for 150 hr)	a_0 = 8.799Å[36] c_0 = 4.544Å(for FeCr) a_0 = 9.188[36] c_0 = 4.812(for FeMo)	Mo 11	Cr 29	Fe 55	Ni 5	FeCr[36] FeMo[36] Fe(CrMo)[36]			
				$(Fe, Ni)_x(Cr, Mo)_y$				Mo 8.35	Cr 30.84	Fe –	Ni 4.1[11]
Chi (χ)	bcc α-Mn structure	a_0 = 8.878 ± 0.005	a_0 = 8.920[45] a_0 = 8.878[46] [47] a_0 = 8.862[8] a_0 = 8.89[42]	Mo 22	Cr 21	Fe 52	Ni 5	$Fe_{36}Cr_{12}Mo_{10}$ [44] [45] $(FeNi)_{36}Cr_{18}Mo_4$ [8] $M_{18}C$[24]			
Laves (η)	Hexagonal	a_0 = 4.73 ± 0.01 c_0 = 7.72 ± 0.01	a_0 = 4.744[49] c_0 = 7.725	Mo 45	Cr 11	Fe 38	Ni 6	Fe_2Mo[49]			
Matrix, Austenitic (γ)	fcc	a_0 = 3.598	a_0 = 3.595[8]	Mo 2.66	Cr 17.3	Fe bal	Ni 13.1	Mo 1.99	Cr 16.3	Fe bal	Ni 15.85[8]

be relatively complete in 50 percent cold-work as compared to lesser cold-worked samples.

TEM studies on post cold-work anneal samples are in progress. However, a preliminary examination confirms that the recovery is complete in 50 percent cold-work and partially complete in lower amounts of cold-work. Furthermore, that the precipitate is bulkly in 50 percent cold work and much smaller in size in 20 percent cold-worked samples.

B. 304 Stainless Steel [J. Moteff, V.K. Sikka, H. Nahm and R.V. Bhargava]

Presently work on 304 stainless steel is involved in the following areas.

1. The Determination of Ultimate Tensile Strength of AISI 304 Stainless Steel from Hot-Hardness Measurement.
2. TEM Study of 16 Different Heats of 304.
3. Tensile-Substructure Correlation of 304L Stainless Steels tested at temperatures up to 1375°C.
4. Characteristics of Cracks Formed as a Result of Plastic Deformations at Elevated Temperatures.

1. The Determination of Ultimate Tensile Strength of AISI 304 Stainless Steel from Hot-Hardness Measurement - Work has been completed on hot-hardness of 16 different heats of 304 stainless steels. The correlation of hot-hardness data with hot-tensile, only nine sets of data, is presented in this report.

Recently Cahoon[4] presented an improved equation relating hardness to ultimate strength of metals and alloys. This equation is given as:

$$\sigma_u = \frac{H}{2.9}\left(\frac{n}{0.217}\right)^n \quad (2)$$

where σ_u is the ultimate nominal stress, H is the Vickers Pyramid Hardness and n the strain hardening coefficient as related to the familiar equation,

$$\bar{\sigma} = k\bar{\varepsilon}^n \quad (3)$$

with $\bar{\sigma}$ and $\bar{\varepsilon}$ being the true stress in the plastic region and the true strain, respectively. The constant k is generally called the strength coefficient.

The improved equation is based on the earlier work (1951) of Tabor[5], which had the following form:

$$\sigma_u = \frac{H}{2.9}(1-n)\left(\frac{12.5n}{1-n}\right)^n \quad (4)$$

where the parameters are the same as those used for Equation (2) and σ_u and H given in the same units of kg mm^{-2}.

In another article, Cahoon et al.[6] showed a reasonable correlation of the calculated yield strength (0.2 pct offset) with hardness measurements using the expression,

$$\sigma_y = \frac{H}{3}(0.1)^n \quad (5)$$

for the metals brass and steel in either the cold rolled or tempered condition; and aluminum alloys in either the cold rolled or aged condition. The strain hardening parameter n may be obtained from the Meyer's hardness coefficient m by

the relationship,

$$n = m-2 \tag{6}$$

an equality which has been shown to be valid theoretically and confirmed experimentally[5].

The result of the present work is used to show the degree of agreement between the calculated ultimate stress levels of seven to nine different heats of AISI 304 stainless steel tested in tension at temperatures of RT, 427, 593, and 649°C (RT, 800, 1100, and 1200°F) based on hot-hardness data obtained from samples fabricated from the same respective heats, with the actual experimental test results. About 30 test results are compared using specimens which were tensile tested under the above conditions at a strain rate of approximately 8×10^{-4} sec^{-1}. The details of hot-hardness measurement technique have already been described in the previous report.[7]

As pointed out by Cahoon[4], if it is accepted that the true stress on a stress-strain curve at a strain of 0.08 is given approximately by H/2.9 as suggested by Tabor[5] and supported by Cahoon et al.[6], then the relationship given as Equation (2) is developed from Equation (4). Actually, Tabor[5] suggested values of the constant in the denominator to lie in the range of 2.9 to 3.0 with the lower value for steel and the higher value for copper, while Cahoon et al.[6] showed values of 3.0 ± 0.1 for steel and aluminum specimens. The value of

the constant for the present study on 304 stainless steel at the elevated temperatures was found to be 3.1 $\pm$ 0.2, in reasonable agreement with the 2.9 and 3.0 values suggested previously.

Accordingly, the following equation,

$$\sigma_u = \frac{H}{3.1}\left(\frac{n}{0.217}\right)^n \qquad (7)$$

was used in the present comparisons of the relationship of ultimate strength with hardness values as shown in Figure 11. The symbols, designated as specimen numbers, represents the hot-hardness results, at the four temperatures, of a sample taken from the button-head of the room-temperature tensile specimen. The ultimate strength values were taken from four different specimens of the same respective heats.

Using average values for the strain hardening coefficient, n, of 0.40 $\pm$ 0.03, 0.41 $\pm$ 0.03, 0.36 $\pm$ 0.04 and 0.30 $\pm$ 0.02 for specimens tested at the temperatures: RT, 427, 593 and 649°C respectively, and Equation (7) the calculated ultimate strength is compared with the actual experimental ultimate strength for each condition of material (heat) and temperature as shown in Figure 12. With the exception of the 427°C test conditons where the average error was 6.2 percent, most of the calculated values fell within 5 percent of the corresponding experimentally determined ultimate strength, being 4.5, 3.9 and 3.5 percent, respectively, for the RT, 593 and

649°C test conditions.

Figure 13 clearly leads one to conclude that the calculated values of the 0.2 percent offset yield strength is underestimated when using Equation (5), especially for the case of the seven room temperature values shown at the higher stress levels. The calculated yield strengths for the case of the 593°C test conditions were within 1 percent of the experimental values and those for 649°C being within 7 percent. The calculated room temperature yield strengths were low by an average of 24 percent and those of the 427°C test condition by 19 percent. A constant of 3.1 was also used for the calculation of the yield strength.

The present studies show that similar to the correlation of the room temperature ultimate strength levels with hardness values as presented by Tabor[5] and Cahoon[4,6], the elevated tensile properties may be obtained from corresponding hot-hardness measurements. Equation (7), differing only by a constant from Equation (2) shows excellent agreement for test temperatures up to 649°C. The calculations of the yield strength appears to be reasonable for only the higher test temperatures.

It is interesting to note that the average diameters of dislocation cells (subgrains), which are formed in tensile tests of AISI 316 stainless steel specimens[8] do not change

significantly in the test temperature range of 200 to 650°C. In addition, the strain hardening coefficient values are shown to vary inversly with the subgrain dimensions[9]. The substructure characteristics, which are important parameters in the correlation of hardness with tensile strengths, are presently being evaluated with the use of a 200 kV transmission electron microscope. In particular, the dislocation arrangements in the region of the hardness indent and in the gage section of a tensile specimen strained to a value of about 8 percent are being studied.

2. TEM of 16 Different Heats of 304 - Transmission electron microscopy on the button-head region of tensile specimens of 8 of the 16 different heats of 304 stainless steel have been completed. Some of the representative micrographs are presented in Figure 14 and 15. Stacking fault energy measurements are being made from these micrographs and will be related to the chemical variation.

3. Tensile-Substructure Correlation of 304L Stainless Steel Tested at Temperatures up to 1375°C - Substructure studies were initiated on a set of annealed type 304L stainless steel sheet specimens which have been tensile tested[7] in the temperature range of 25 to 1375°C. Samples, 2.65 (0.1") mm squares, were cut near the fracture end and electropolished for TEM examination. The TEM observations have been concentrated on cell, subgrain and mobile dislocation line density measurements. Re-

sults obtained up to date are listed in Table III. Since TEM samples were taken from various portions of the gage length, the cross-sections were measured and corresponding true stress values calculated. These values are also reported in Table III.

Typical substructures observed for specimens tested from 25 to 600°C are shown in Figure 16. At room temperature (25°C) planar slip is the predominant mode of deformation and high dislocation density areas observed lie along the {111} traces, Figure 16a. At higher temperatures, dislocation cells whose walls are composed of massive dislocation tangles are observed. The average cell intercepts increase gradually with increasing temperature and decreasing tensile strength, Table III.

The substructure developed at test temperatures of 800 and 1000°C are shown in Figure 17. A comparison of Figure 17 with lower test temperatures (< 600°C), Figure 16 shows the rearrangement of cell boundaries into well defined subgrains. The subgrain intercept increases with test temperature and decreasing tensile strength. The mobile dislocation line density for 800 and 1000°C samples is shown in Figures 17C and D. The formation of well defined subgrains at high temperature results in decreasing the mobile dislocation line density. Stacking fault ribbons also become evident for test temperatures of 800 and 1000°C, Figure 17D, point A.

Details of dislocation cell and subgrain intercept and

TABLE III

SUBSTRUCTURE AND TENSILE DATA ON TYPE 304L STAINLESS STEEL

Specimen Number	Test Temperature °C	Elongation At Rupture[b] ϵ_R, Percent	Tensile Strength		Hardness DPH[e]	Reduction In The Area At The Foil Plane Percent	True Stress At The Foil Plane		Average Subcell Or Subgrain Intercept μm	Average Mobile Dislocation Density cm^{-2}
			Kg mm^{-2}	Ksi			Kg mm^{-2}	Ksi		
10	25	64	66.5[c]	94.6	174	36.7	105.0	149.4	-	-
11	200	38	47.2	67.1	227	25.5	63.3	90.0	0.52	-
13	600	34	33.9	48.2	218	16.5	40.6	57.8	0.60	-
15	800[a]	52	13.0[d]	18.5	170	42.9	22.8	32.4	0.77	3.14×10^9
16	1000	44	5.0	7.1	145	12.0	5.7	8.1	1.49	1.70×10^9
17	1200	53	2.1	3.0	127	13.7	2.4	3.4	-	-
18	1300	48	1.3	1.9	110	9.1	1.4	2.0	-	-
19	1350	41	0.91	1.3	104	6.0	1.0	1.4	-	-
20	1375	43	0.86	1.2	107	5.6	0.9	1.3	-	-

(a) Tests from 800 to 1375°C were performed in an Argon atmosphere.

(b) Based on a 0.076 cm thick sheet specimen with a 2.54 cm gage length.

(c) Strain rate in air, 8.2×10^{-5} sec^{-1}.

(d) Loading rate in argon 0.15 cm/min (Cross head speed).

(e) After test; 1 Kg load.

mobile dislocation density with tensile strength is in progress, and will be presented in the next report.

4. Characteristics of Cracks Formed as a Result of Plastic Deformations at Elevated Temperatures - Plastic Deformation involves deformation within the grains and sliding between the grain boundaries. The grain boundary sliding becomes a very important parameter especially in the high temperature plastic deformation. Optically microscopy study is in progress to investigate the contribution of grain boundary sliding to the total deformation in the ORNL tensile specimens (9T2796) tested at 1200°F. The experimental data and the discussions on the microcracks formed in tensile tested specimens have been included in the previous progress reports[7].

The experimental technique adopted by Hensler et al.[10] is employed for the study of grain boundary sliding. In this technique, the maximum longitudinal and transverse length of individual grains is measured with respect to the stress axis. The generation of raw data on six tensile specimens of 304 stainless steel has been completed and the detailed analysis is underway. The experimental data and computer analysis will be presented in the forthcoming reports.

The future work will also continue on optical microscopy study on microcracking of tensile specimens (9T2796), tested under a wide range of stress levels and test temperature.

C. Incoloy 800 [C.C. Yu]

Substructure of Incoloy 800 tensile tested at 800, 1000, 1200, 1300 and 1400°F at a constant strain rate of 4×10^{-4} sec^{-1} have been completed. Typical micrographs of the dislocation line density in button-head of the specimen I-1 are presented in Figure 18. The cell and subgrain formation at temperatures in the range 1000-1400°F are shown in Figure 19. The summary of the substructure properties of Incoloy 800 resulting from short term tensile tests are given in Table IV.

The formation of dislocation cells or subgrain is dependent on the test temperature. At low temperature, only dislocation cells were observed. At 1200°F dislocation cells were observed to transform into well defined subgrains.

The dislocation cell or subgrain intercept is strongly stress dependent. The data on Incoloy 800 is plotted as a function of ultimate tensile stress in Figure 20. The dislocation cell intercept have a stress dependence of -2, and the subgrain intercept -1. Such a stress dependency is similar to that observed for 316 stainless steel[8] and on creep of 304 stainless steel[11].

The results from specimen 2-J-34 fall on both lines in Figure 20, which suggests that the test conditions might be critical for transition of dislocation cells into subgrains.

In all Incoloy 800 samples dislocation densities were

TABLE IV

SUBSTRUCTURE DATA ON INCOLOY 800 RESULTING FROM SHORT TERM TENSILE TESTS[a]

Test	Specimen Number	Temperature °F	Temperature °C	Tensile Strength, σ_{UTS} Ksi	Tensile Strength, σ_{UTS} Kg mm^{-2}	Time To Fracture Hours	Average Subgrain Intercept	Mobile Dislocation Density, cm^{-2}
1	I-1[b]	800	427	78.7	55.4	0.58	0.278[d] (6)[e]	N.M[f]
2	2-K-11[c]	1000	538	63.2	44.5	0.43	0.340[d] (6)	1.77×10^{10} (1)
3	2-J-34[c]	1200	649	51.9	36.5	0.62	0.701 (11)	N.M
4	2-0-15[c]	1300	704	40.7	28.6	0.50	1.075 (7)	N.M
5	2-B-2[c]	1400	760	31.2	22.0	0.71	1.004 (24)	2.69×10^{9} (2)

(a) $\dot{\varepsilon}_t = 4 \times 10^{-4}$ sec^{-1}, True axial strain rate.

(b) Grade 1 (Mill-Annealed) Bar Stock.

(c) Grade 2 (Solution-Annealed) Bar Stock.

(d) Dislocation cells only. All other points are for either both cells and subgrains or only subgrains.

(e) Number in parenthesis represents the number of photographic plates used for that determination.

(f) Not possible to measure.

very high. In most of the cases it was not possible to make counts on individual dislocations. Some measurements on small areas of the samples were possible and preliminary relationship between dislocation density and ultimate tensile stress is presented in Figure 21. Although only two data points are available, a line with stress dependency of two still shows reasonable agreement.

The present substructure data on Incoloy 800 suggests that its behavior can be compared closely with 304 or 316 stainless steels.

D. Nickel 270 [J. Stubbins]

Specimens from an investigation of steady-state creep in Nickel 270 were obtained for microstructural examination using TEM. The creep behavior has been reported[12] and values for the creep activation energy, Qc, and the stress exponent, n, were given. The arrows on a graph from that publication, Figure 22, indicate which specimens are presently on hand for TEM examination, and others could be obtained for further investigation. A specimen preparation method for TEM studies has been developed. A study to examine the correlation between creep properties and substructural features will be carried out.

IV. PLANS FOR FUTURE WORK

The substructure of 316 stainless specimens tested at 1350°F

in the change-in-stress experiment will be evaluated. These results will be compared to similar studies conducted at a lower temperature.

Work will continue on the recovery characteristics of cold-worked 316 stainless steel with particular emphasis on the studies of precipitate characteristics and dislocation substructure.

Hot-hardness measurements will be made on 304 stainless steel specimens having different subgrain dimensions. The results will be compared to similar studies performed at room temperature which suggest that the constant k in the Petch-Hall type relationship

$$H = H_i + k\, d^{-1/2}$$

also varies with the subgrain size.

Grain boundary sliding contributions to total specimen strain in deformed 304 stainless steel will be completed for tests performed at one temperature and six strain rates.

TEM evaluations of the heat-to-heat set of 304 stainless steel specimens will be continued. Stacking fault energies and other substructural characteristics will be correlated with the reported mechanical properties of these alloys.

Preliminary TEM studies on Incoloy 800 and Nickel 270 will continue.

REFERENCES

1. J. L. Kamphouse, J. C. Blake and J. Moteff, Rev. Sci. Instr., 40, 321 (1969).

2. B. Weiss and R. Stickler, Met. Trans., 3, 851 (1972).

3. J. E. Spruiell, J. A. Scott, C. S. Ary and R. L. Hardin, Met. Trans., 4, 1533 (1973).

4. J. R. Cahoon, Met. Trans., 3, 3040 (1972).

5. D. Tabor, J. Inst. Metals, 79, 1 (1951).

6. J. R. Cahoon, W. H. Broughton and A. R. Kutzak, Met. Trans., 2, 1979 (1971).

7. Progress Report, September - December, 1972, COO-2107-8, March 15, 1972, University of Cincinnati, Cincinnati, Ohio.

8. D. J. Michel, J. Moteff and A. J. Lovell, Acta Met. (In Press).

9. K. D. Challenger and J. Moteff, Scripta Met., 6, 155 (1972).

10. J. H. Hensler and R. C. Gifkins, J. Inst. Metals, 92, 340 (1963-64).

11. C. C. Yu, M.S. Thesis, Univ. of Cincinnati, Cincinnati, Ohio (1973).

12. E. C. Norman, S. A. Doran, Acta Met., 18, 723 (1970).

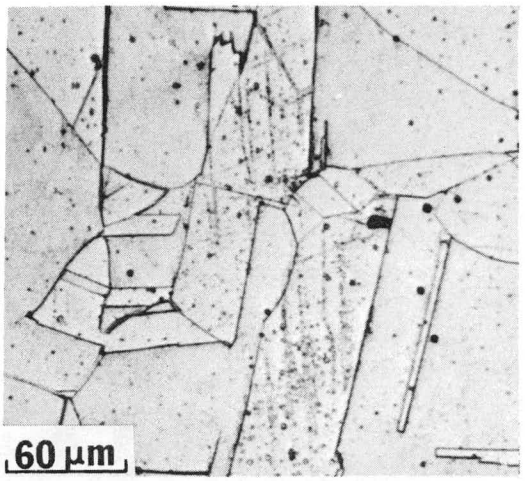

FIGURE 1

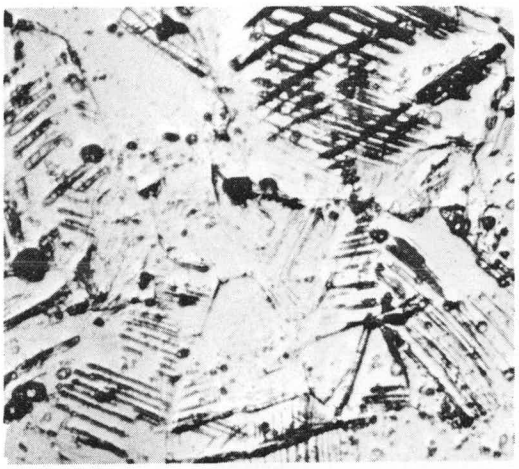

FIGURE 2

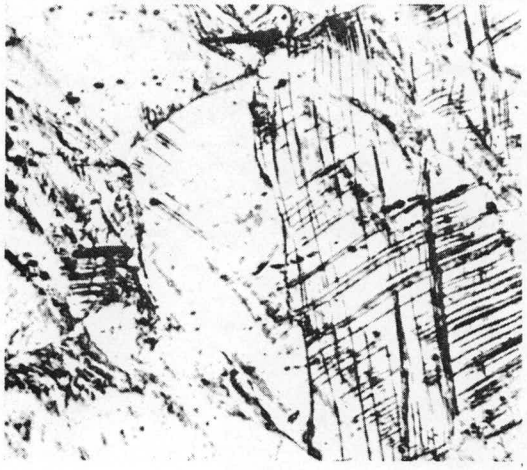

FIGURE 3

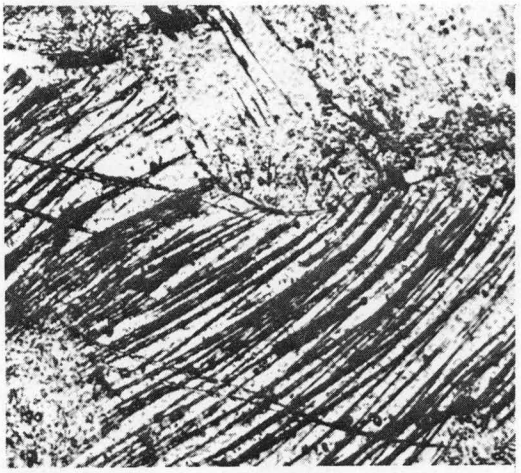

FIGURE 4

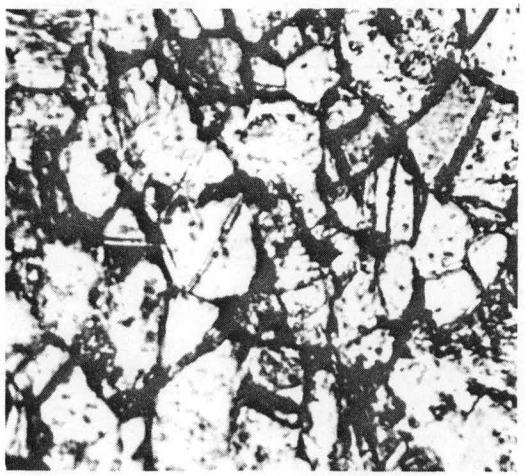

FIGURE 5

MICROSTRUCTURES OF 316 STAINLESS STEEL SHOWING:

Fig (1) Annealed 316 SS Bar
Fig (2) 20% C.W. 316 SS Bar
Fig (3) 35% C.W. 316 SS Bar
Fig (4) 50% C.W. 316 SS Bar
Fig (5) 20% C.W. 316 SS Sheet

FIGURE 6

HOT HARDNESS VERSUS ANNEALING TEMPERATURE
FOR ANNEALED 316 STAINLESS STEEL

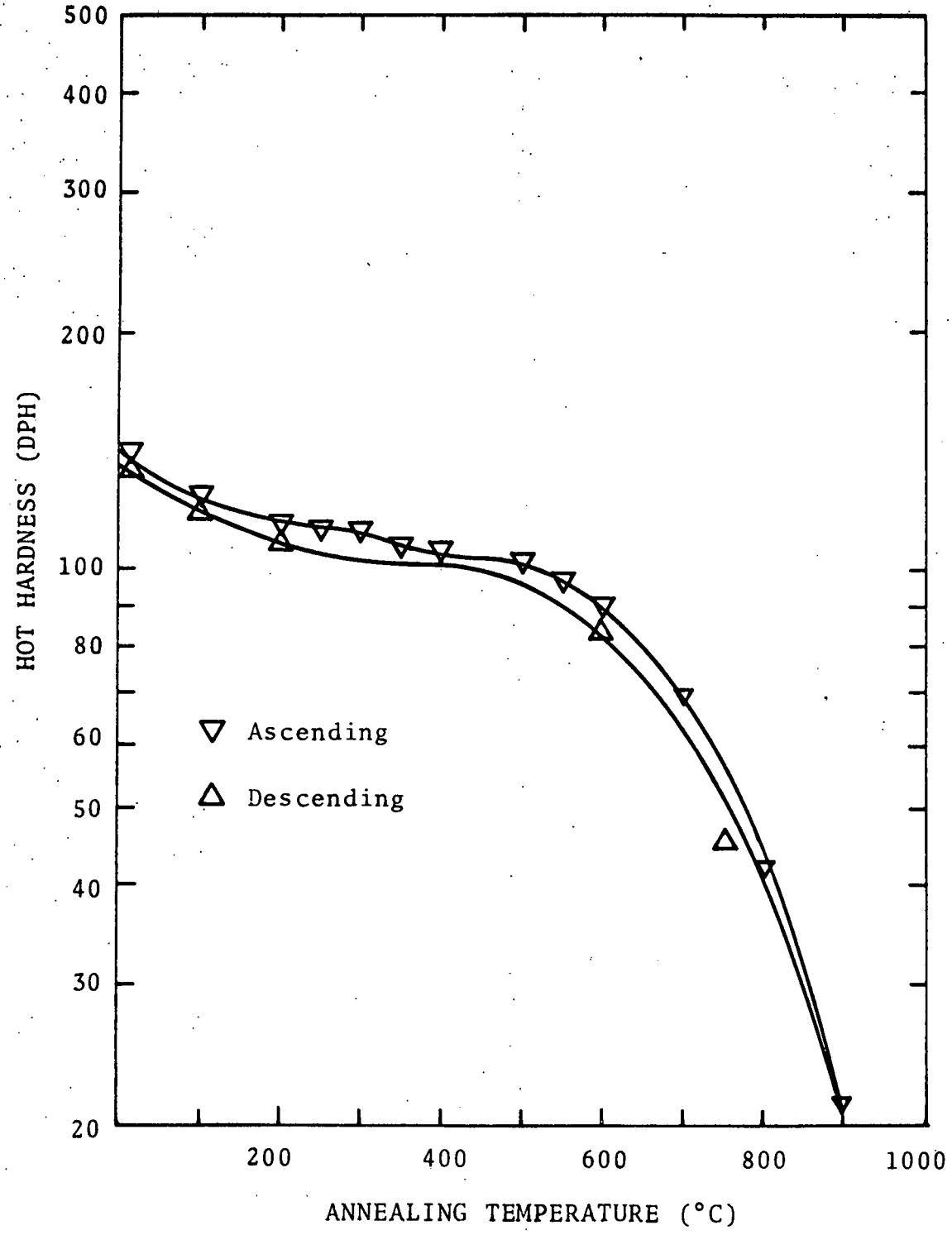

FIGURE 7

HOT HARDNESS VERSUS ANNEALING TEMPERATURE
FOR 20 PERCENT COLD-WORKED 316 STAINLESS STEEL

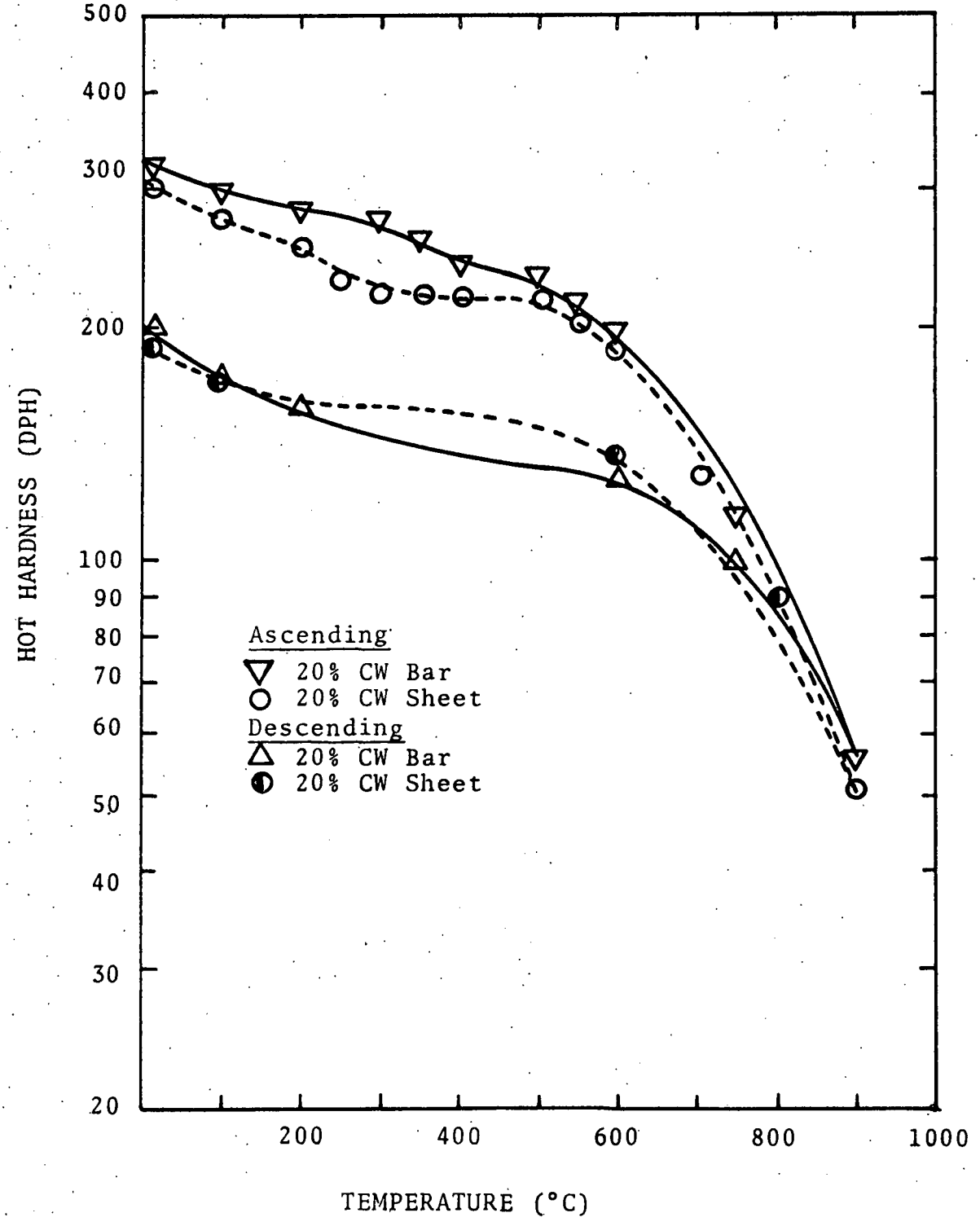

FIGURE 8

HOT HARDNESS VERSUS ANNEALING TEMPERATURE
FOR COLD-WORKED 316 STAINLESS STEEL

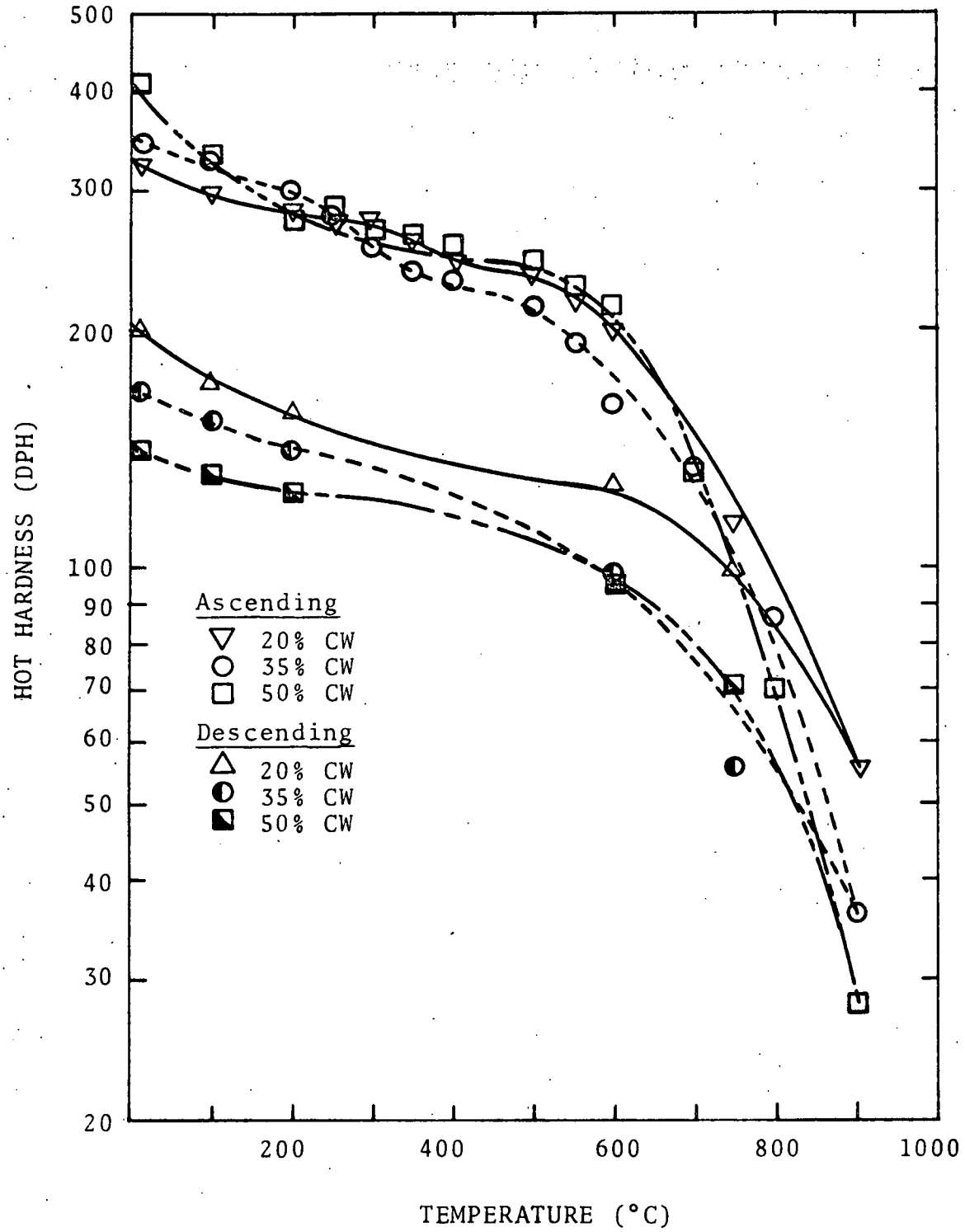

FIGURE 8a

VARIATION OF PERCENT RECOVERY AS A FUNCTION OF PERCENT COLD-WORK FOR AISI 316 STAINLESS STEEL

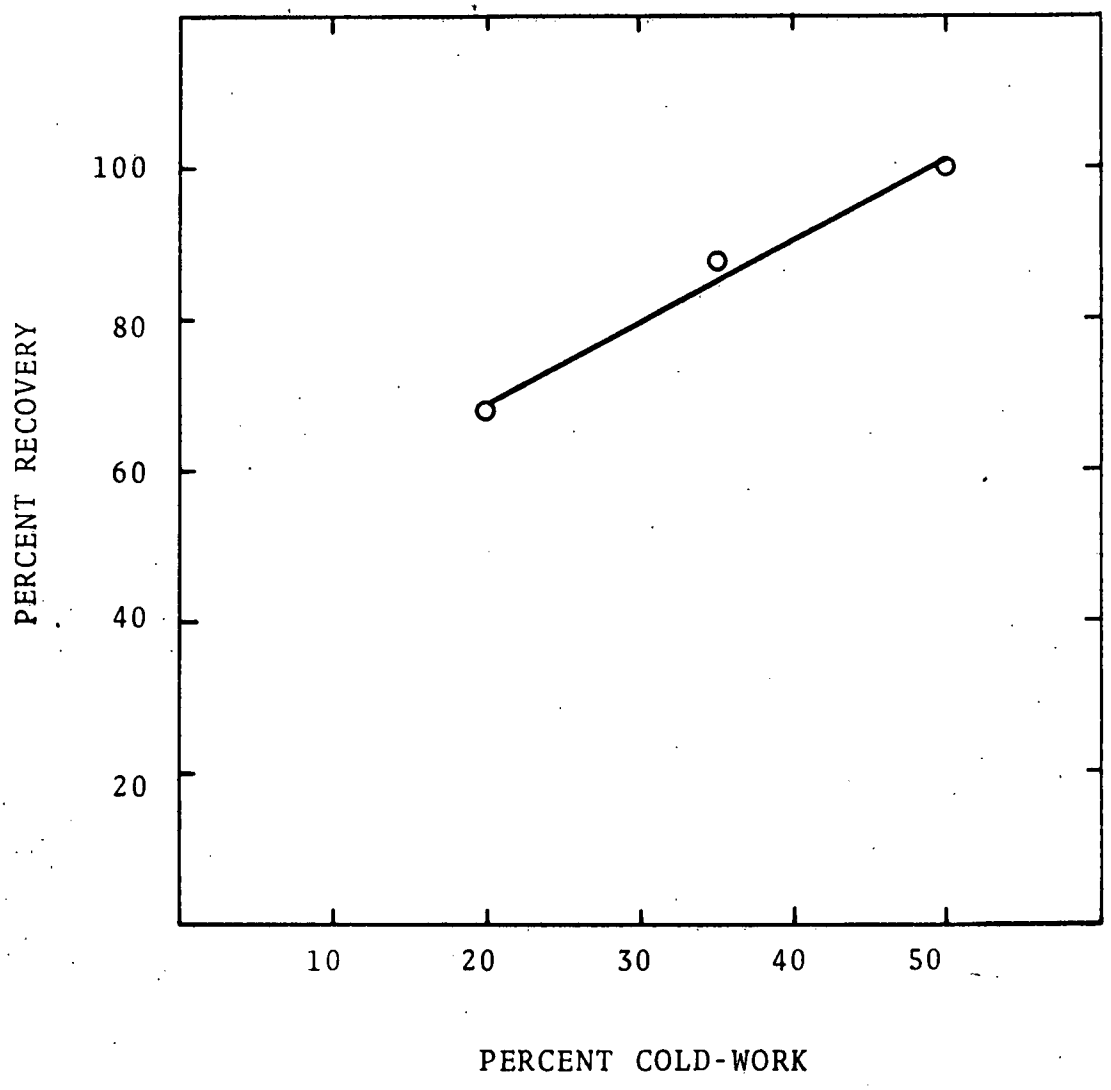

FIGURE 9

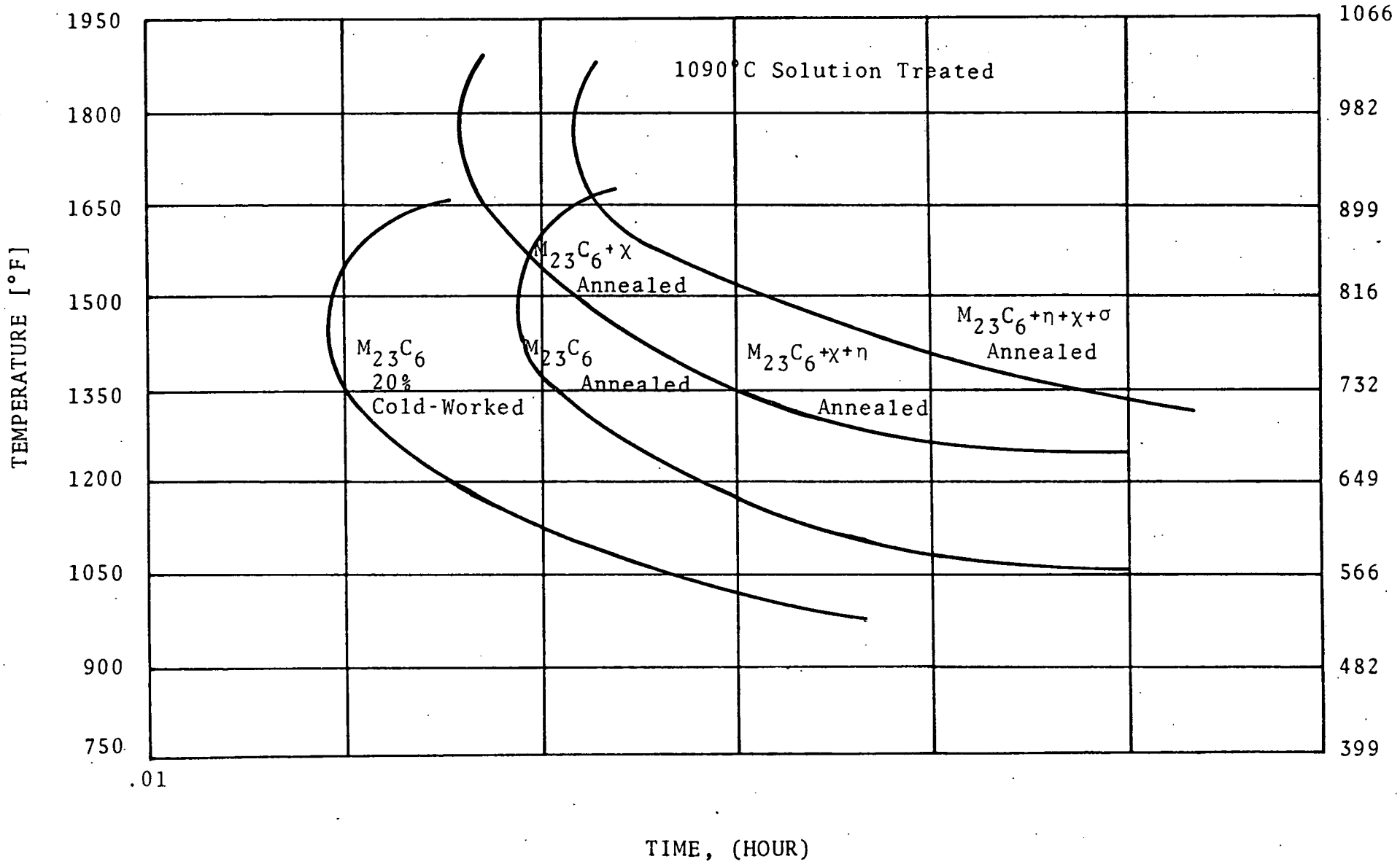

TIME-TEMPERATURE DIAGRAM OF 316L STAINLESS STEEL SHOWING PRECIPITATE PHASE FORMATION AND THE ACCELERATION OF PRECIPITATION WITH THE INFLUENCE OF COLD-WORK (REF. 2)

FIGURE 10

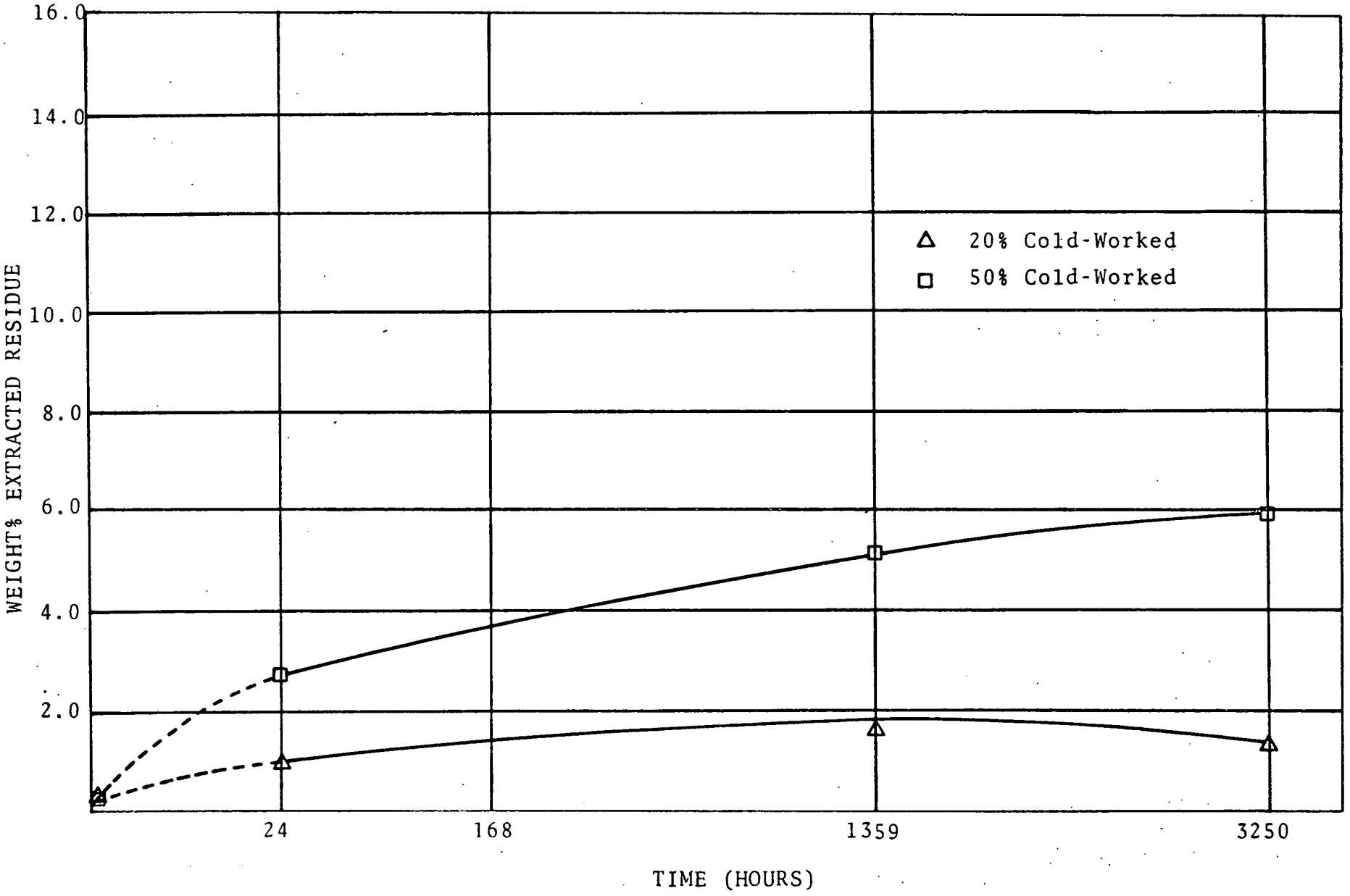

BULK RESIDUE EXTRACTED VERSUS AGING TIME IN 316 STAINLESS STEEL AGED AT 710°C (REF.3)

FIGURE 11

RELATION OF ULTIMATE STRENGTH TO HARDNESS AND STRAIN HARDENING COEFFICIENT FOR AISI 304 STAINLESS STEEL. HARDNESS AND STRENGTH DETERMINATIONS MADE AT THE SAME TEMPERATURE.

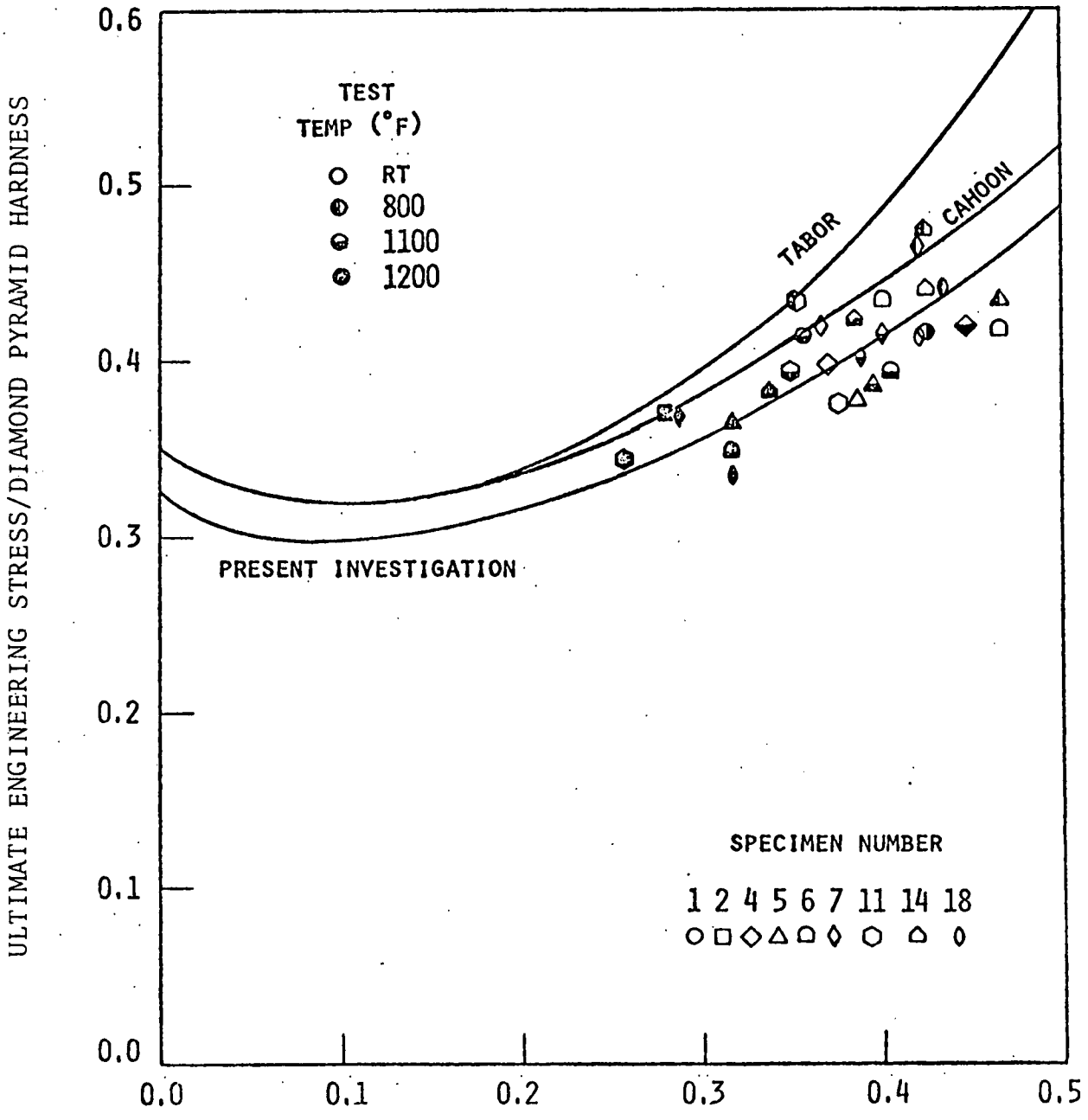

FIGURE 12

COMPARISON OF CALCULATED AND EXPERIMENTAL ULTIMATE TENSILE STRENGTHS FOR AISI 304 STAINLESS STEEL. DATA SYMBOLS REFER TO HEAT NUMBERS AS SHOWN IN FIGURE 11.

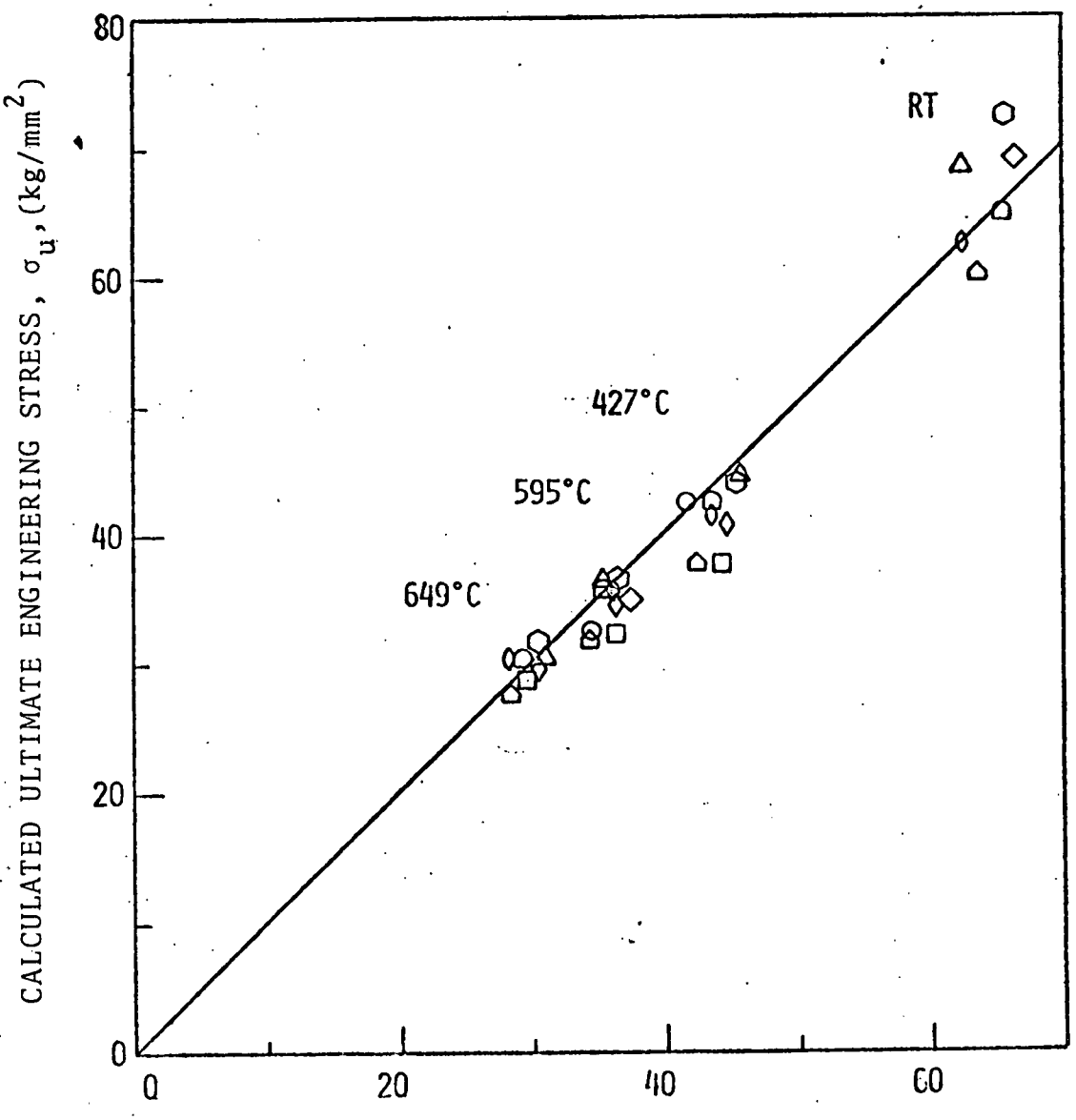

FIGURE 13

COMPARISON OF CALCULATED AND EXPERIMENTAL YIELD STRENGTHS FOR AISI 304 STAINLESS STEEL. DATA SYMBOLS REFER TO HEAT NUMBERS AS SHOWN IN FIGURE 11.

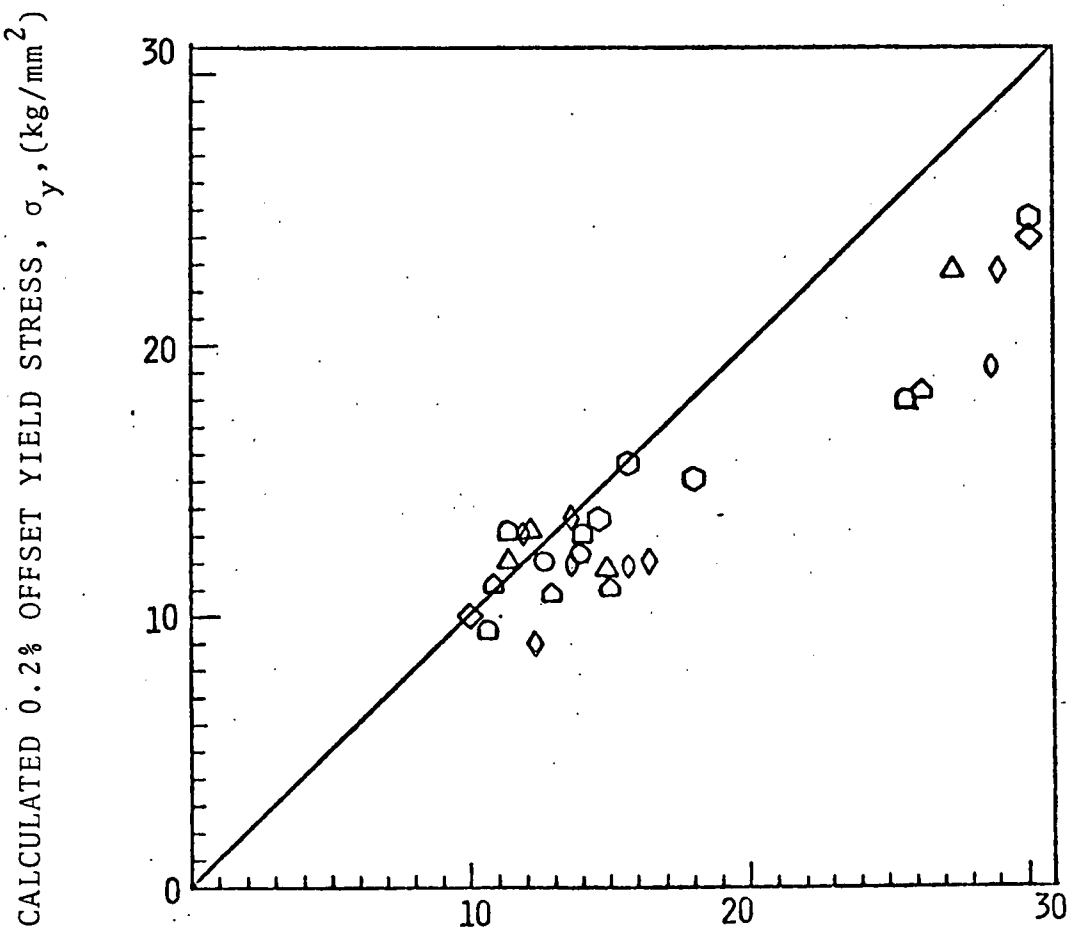

FIGURE 14

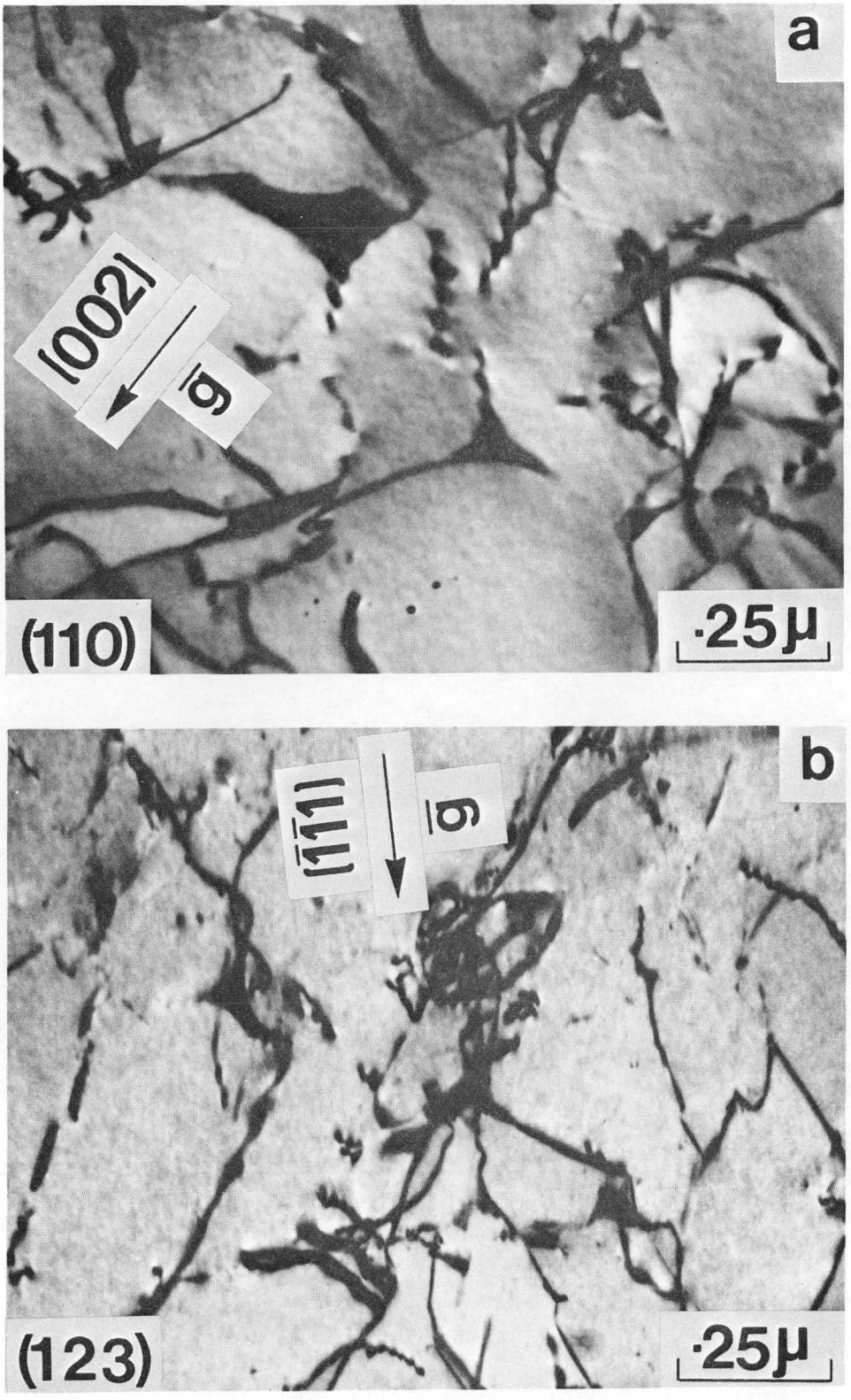

TYPICAL MICROGRAPHS SHOWING ISOLATED EXTENDED NODE FORMATION IN BUTTON-HEAD REGION OF 304 STAINLESS STEEL FOR HEAT NUMBERS, (a) 9T2796 AND (b) 80043813.

FIGURE 15

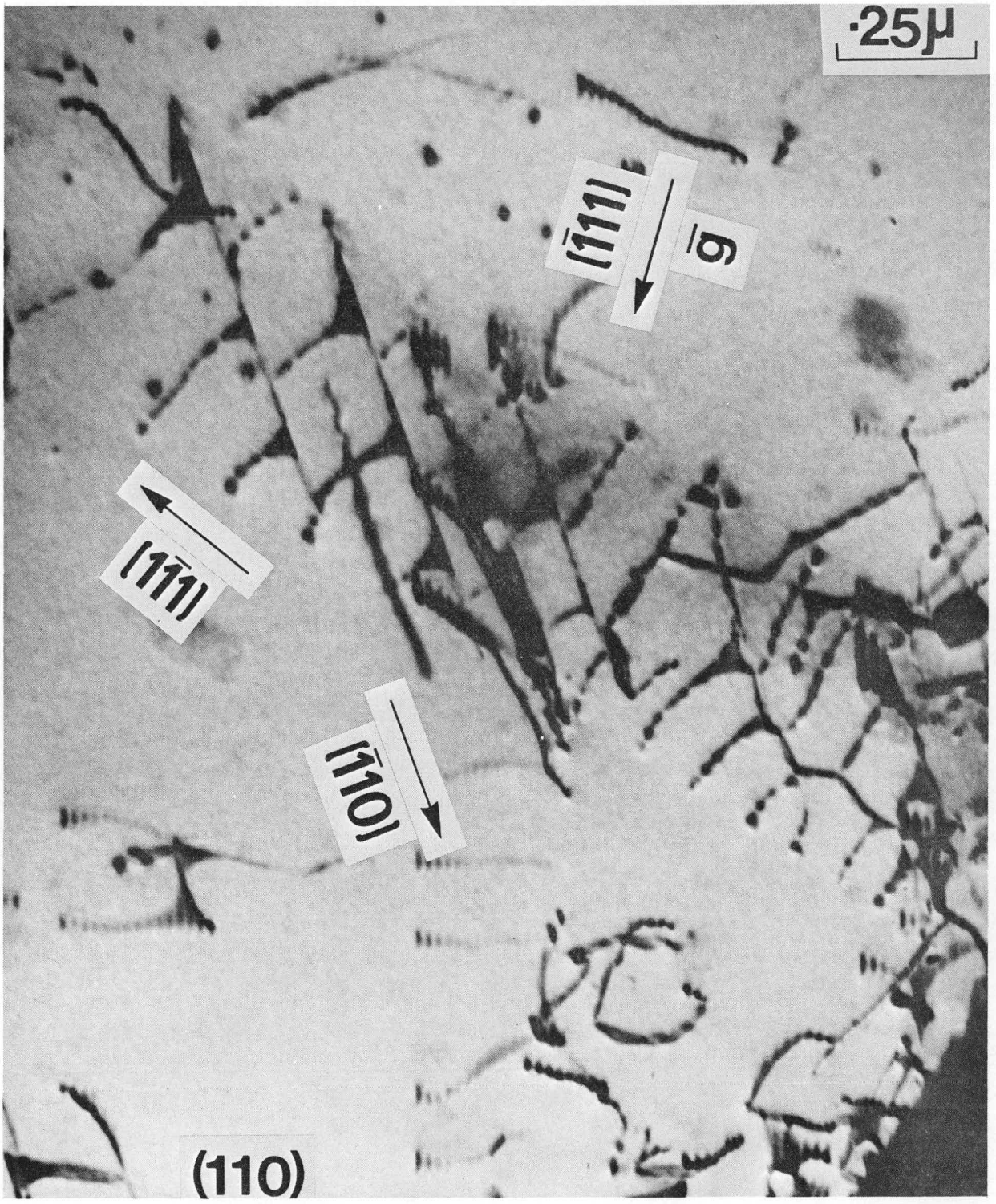

TYPICAL MICROGRAPH SHOWING THE FORMATION OF EXTENDED NODES IN A SLIP BAND IN THE BUTTON-HEAD REGION OF 304 STAINLESS STEEL FOR HEAT NUMBER 346845.

FIGURE 16

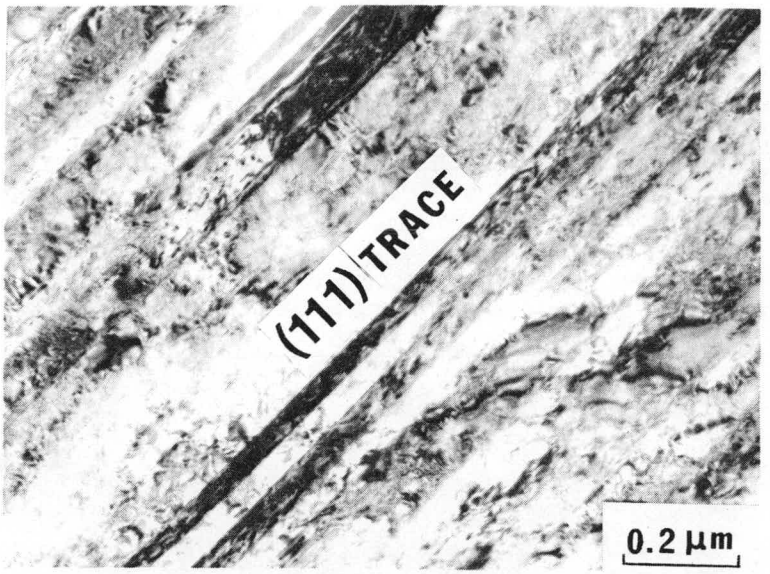

25°C

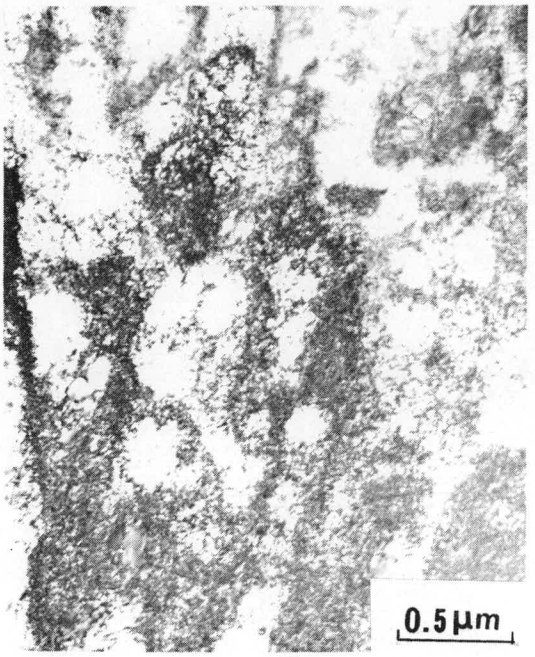

200°C

600°C

MICROGRAPHS OF TYPE 304L STAINLESS STEEL SPECIMENS TENSILE TESTED FROM 25°C TO 600°C SHOWING REPRESENTATIVE DEFORMATION SUBSTRUCTURE.

FIGURE 17

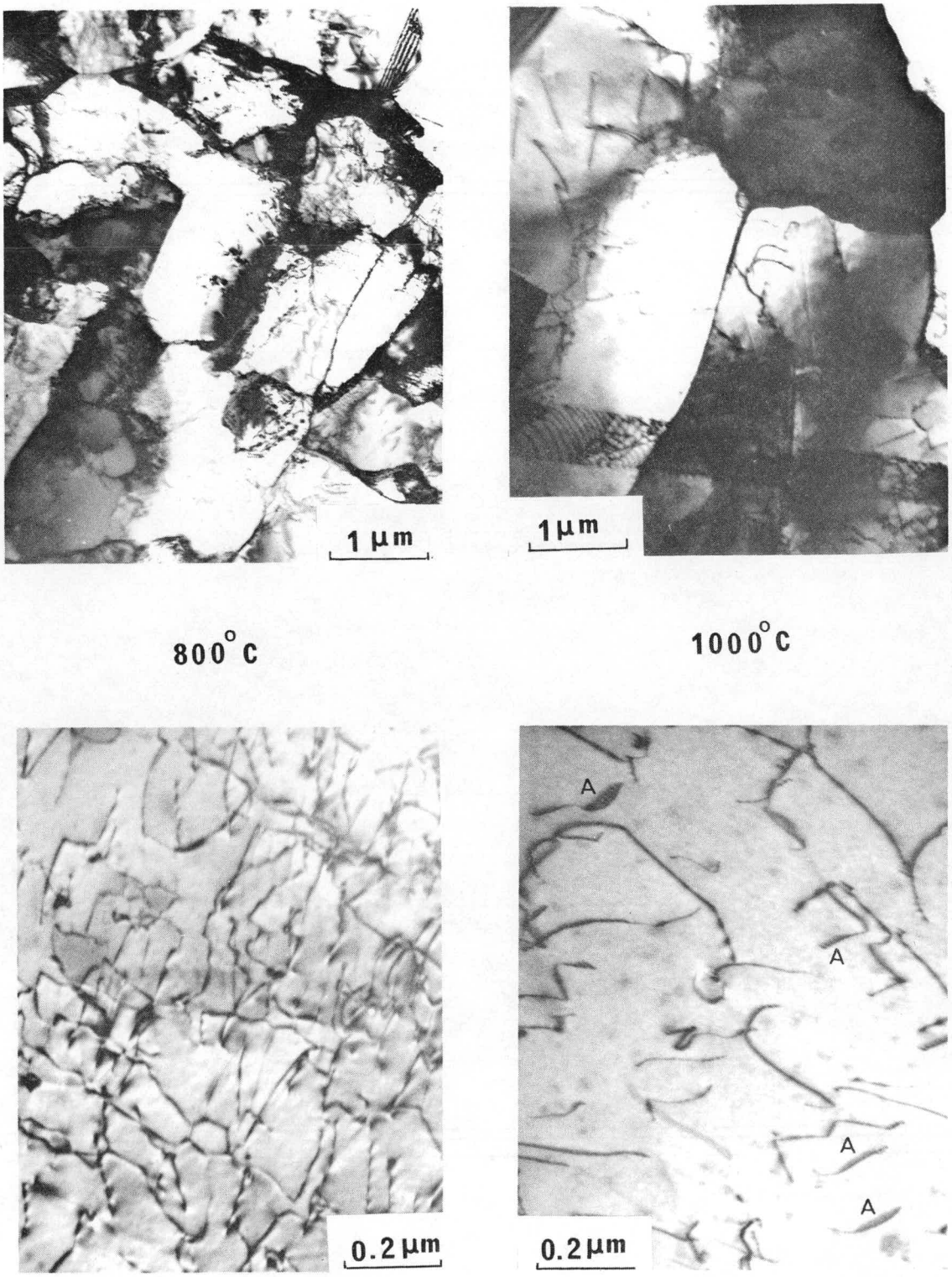

TYPICAL MICROGRAPHS OF TYPE 304L STAINLESS STEEL SPECIMENS TENSILE TESTED AT 800°C AND 1000°C SHOWING SUBGRAINS AND MOBILE DISLOCATIONS INSIDE THE SUBGRAINS

FIGURE 18

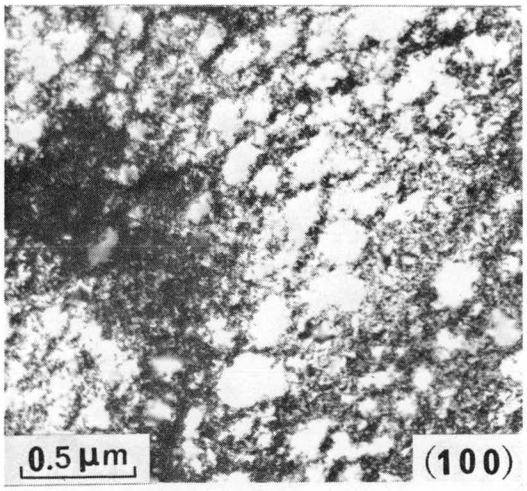

A. 1-1

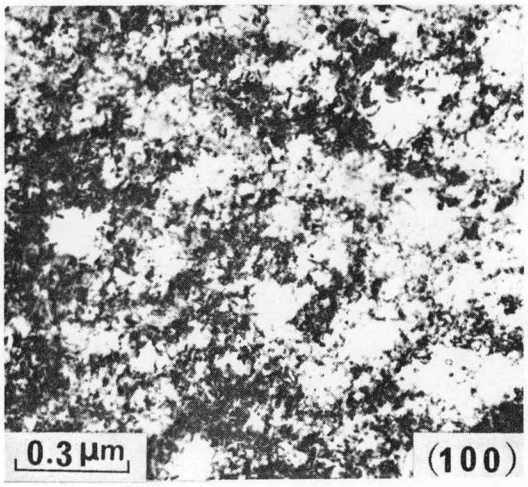

B. 2-K-11

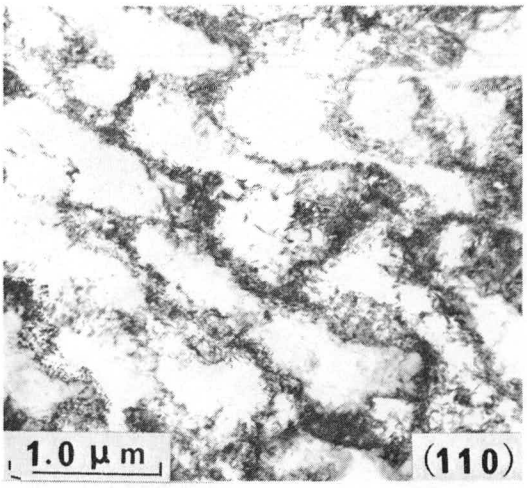

C. 2-J-34

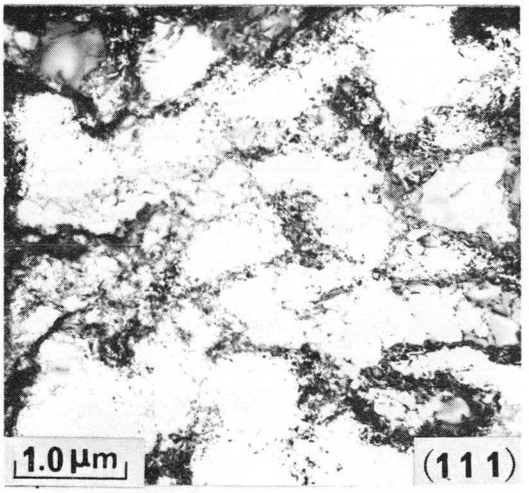

D. 2-0-15

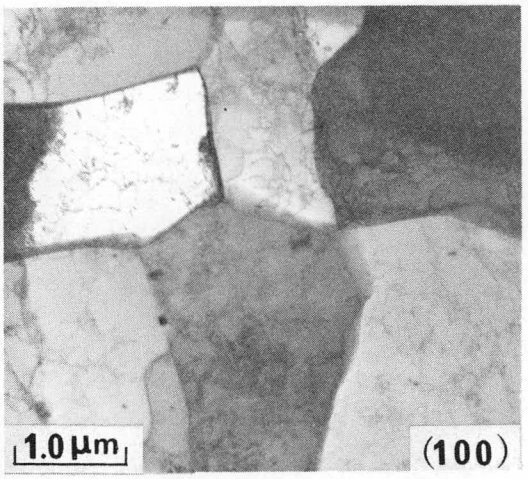

E. 2-B-2

MICROGRAPHS OF INCOLOY 800 SPECIMENS SHORT TERM TENSILE TESTED AT CONSTANT TRUE AXIAL STRAIN RATE OF 4×10^{-4} PER SECOND. SHOWING TRANSITION OF DISLOCATION CELLS TO SUBGRAINS.

FIGURE 19

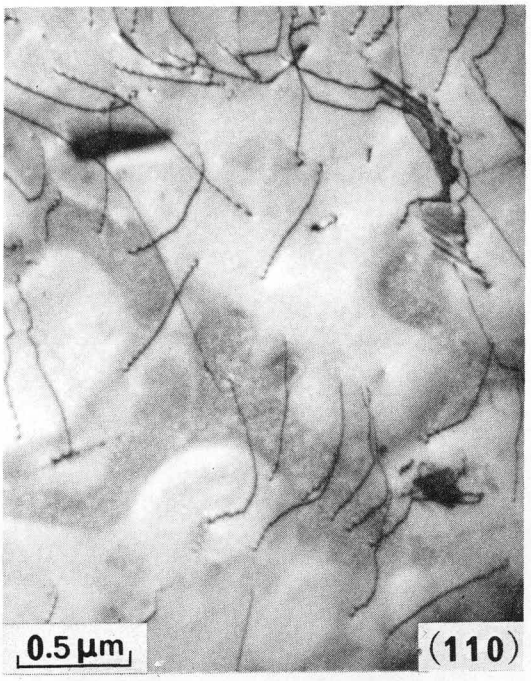

A. UNSTRESS SHOULDER FROM 1-1

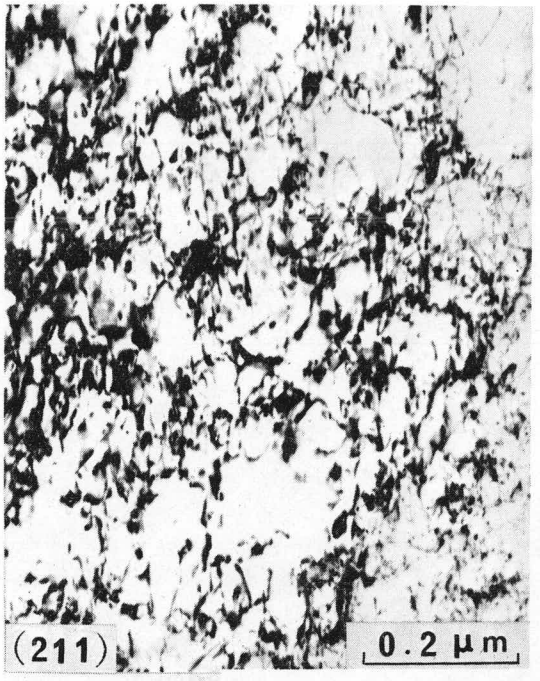

B. 2-K-11

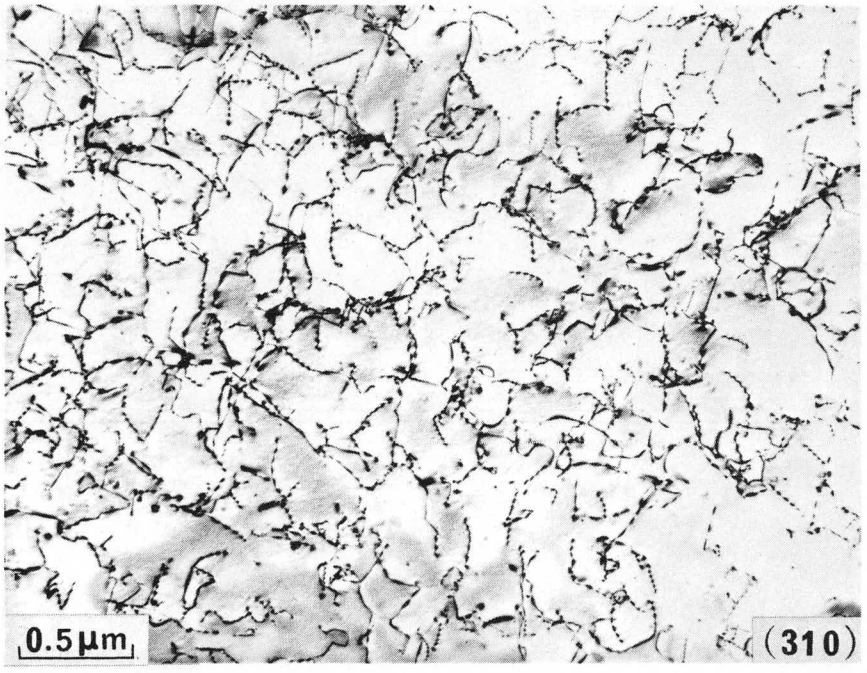

C. 2-B-2

MICROGRAPHS OF INCOLOY 800 SPECIMENS SHORT TERM TENSILE TESTED AT CONSTANT TRUE AXIAL STRAIN RATE OF 4×10^{-4} PER SECOND SHOWING DISLOCATION ARRANGEMENTS.

FIGURE 20

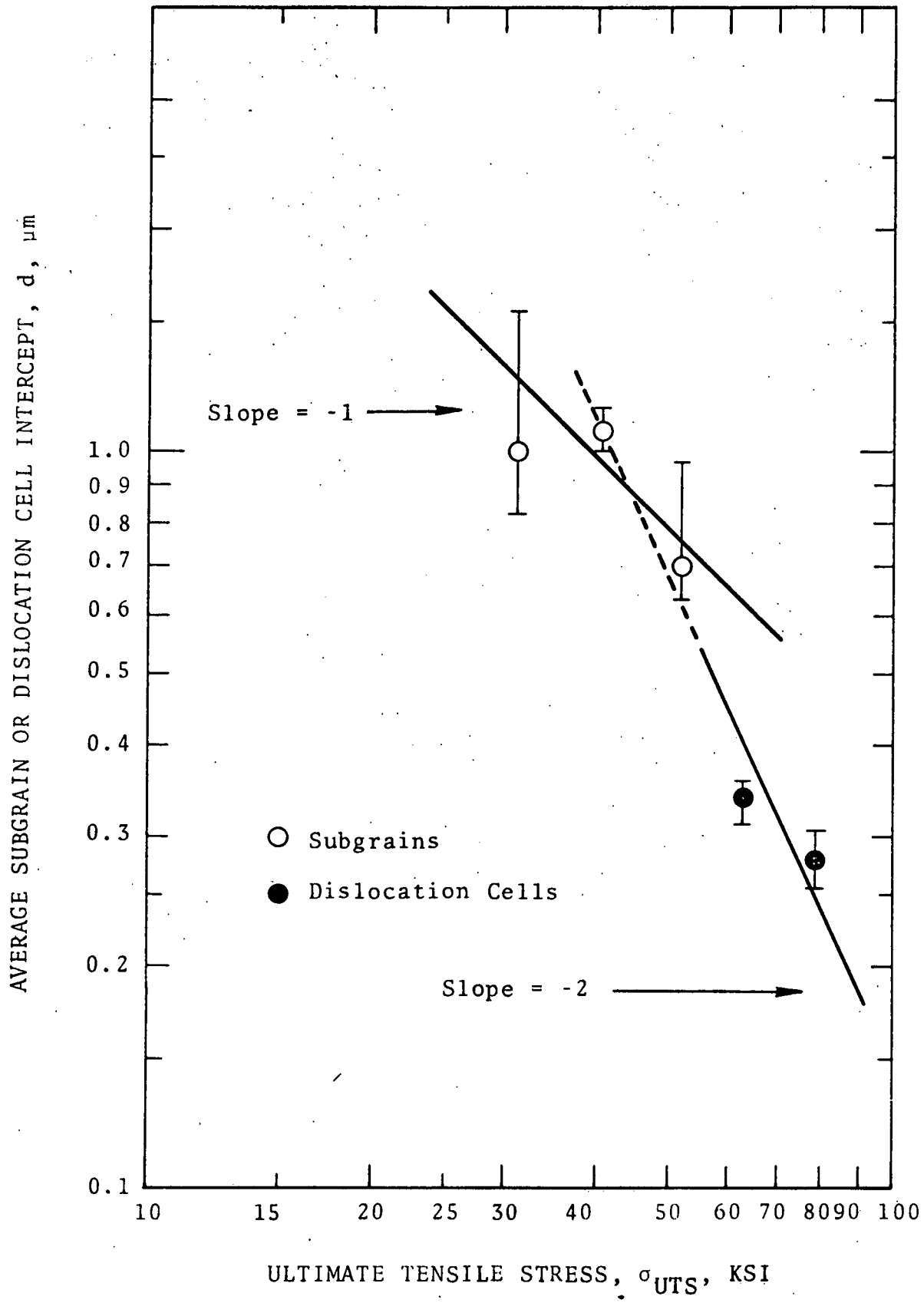

RELATION BETWEEN AVERAGE SUBGRAIN OR DISLOCATION CELL INTERCEPT AND ULTIMATE TENSILE STRESS RESULTING FROM SHORT-TERM TENSILE TESTS OF INCOLOY 800 AT A CONSTANT TRUE AXIAL STRAIN RATE OF 4×10^{-4} sec^{-1}.

FIGURE 21

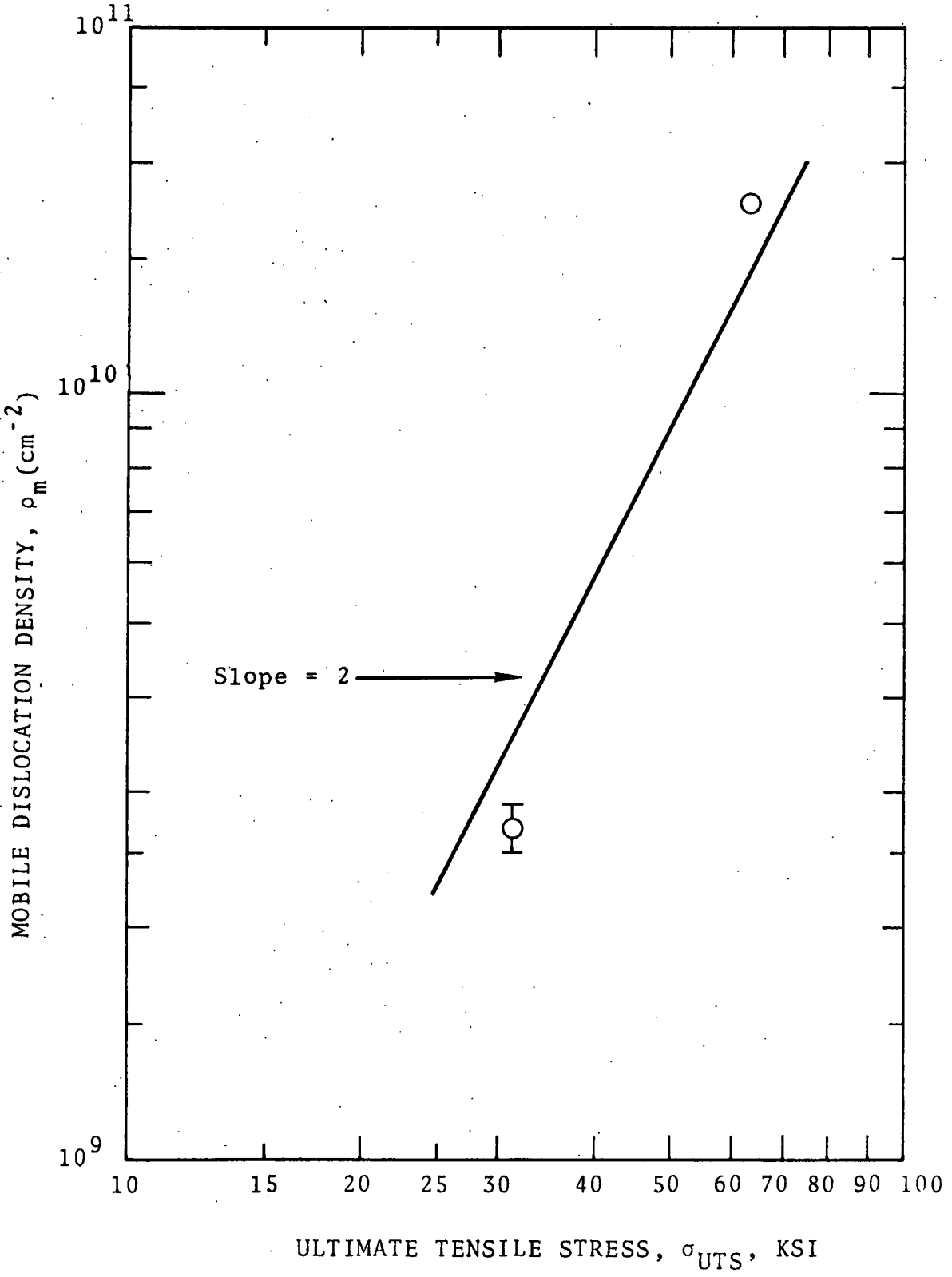

RELATION BETWEEN MOBILE DISLOCATION DENSITY AND ULTIMATE TENSILE STRESS RESULTING FROM SHORT TERM TENSILE TESTS OF INCOLOY 800 AT A CONSTANT TRUE AXIAL STRAIN RATE OF 4×10^{-4} sec^{-1}.

FIGURE 22

LOG_{10} ZENER-HOLLOMAN PARAMETER VERSUS LOG_{10} (STRESS/MODULUS) PLOT FOR NICKEL 270 (FROM REF. 12). ARROWS INDICATE SPECIMENS ON HAND

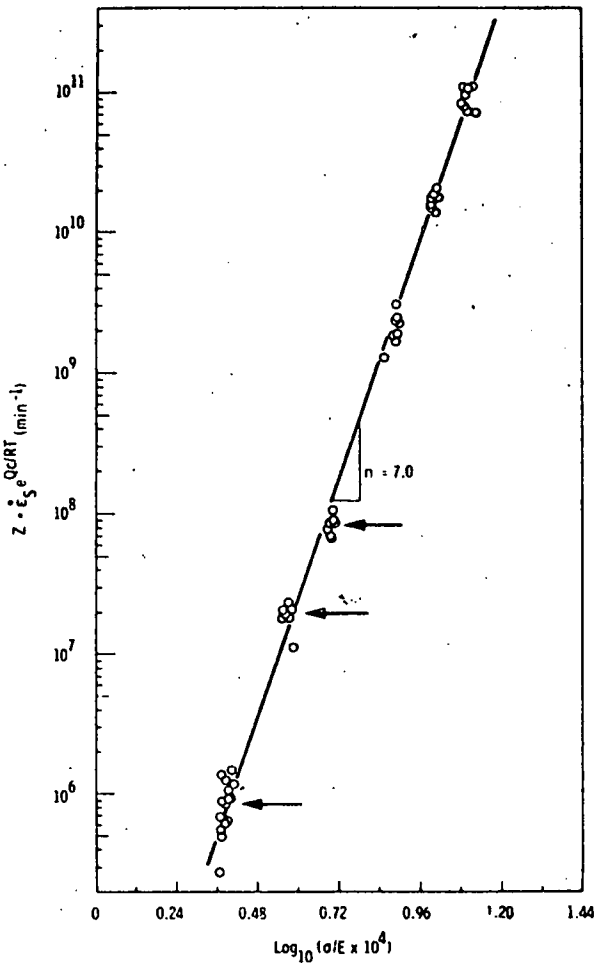

DISTRIBUTION LIST

UNITED STATES ATOMIC ENERGY COMMISSION

Division of Reactor Development and Technology
- Assistant Director for Program Analysis-M. Whitman
- Assistant Director for Program Management-J. W. Crawford
- Assistant Director for Reactor Engineering-E. E. Kintner
- Chief, Fuels and Materials Branch (4)-J. M. Simmons
- Chief, Fuel Engineering Branch-C. E. Weber
- Chief, Coolant Chemistry Branch-B. Singer
- Chief, Reactor Vessel Branch-J. Hunter
- RDT Senior Site Representatives-ANL, ANL-ID, ORNL, Canoga Park Area Office, PNL, G.E.

Division of Naval Reactors-R. H. Steele

Division of Space Nuclear Systems-R. E. Anderson

Division of Research-D. K. Stevens (2)

Division of Technical Information Exchange (5)

Chicago Operations Office-Manager, Patent Office

NATIONAL LABORATORIES

ANL - P. G. Shewmon, B. R. T. Frost, R. Carlander, S. Harkness, R. Weeks, EBR-II Project Associate Director for Materials-Wayne Barney

LMFBR - Program Office

BNL - D. H. Gurinsky, J. Chow

LASL - R. D. Baker

ORNL - W. O. Harms, W. R. Martin, J. R. Weir, E. E. Bloom, R. Swindeman, J. M. Corum

WADCO - T. T. Claudson, J. J. Holmes, J. J. Straalsund, T. Bierlein, L. Blackburn, R. Knecht

PNL - R. Marshall

GOVERNMENT AGENCIES

Albany Metallurgy Research Center - H. Kato

NASA - Lewis Research Center - C. M. Ault

NASA - Washington, D.C. - G. Deutsch

Naval Air Systems Command - R. Schmidt

INDUSTRIAL CONTRACTORS

ANC - C. R. Brinkman

Atomics International - H. Pearlman, D. Kramer, J. Shively

BMI - Columbus - A. Bauer, J. Perrin, C. Jaske

Combustion Engineering - W. P. Chernock

G.E. - Sunnyvale - C. Spalaris, H. Busboom

Gulf General Atomic - J. Howe

Westinghouse - Astronuclear Laboratory - D. C. Goldberg

Westinghouse - Advanced Reactor Division - E. C. Bishop, W. E. Ray, G. Whitlow, A. Boltax

UNIVERSITIES

Ohio State University - J. Spretnak
North Carolina State University - J. R. Beeler, Jr.
University of California, Los Angeles - A. S. Tetelman
University of Florida - F. N. Rhines
Stanford University - O. Sherby
University of Cincinnati - John Moteff
Cornell University - C. Y. Li